Structural essentials for β-*N*-acetylhexosaminidase inhibition by amides of prolines, pipecolic and azetidine carboxylic acids

A. F. G. Glawar,[a,b] R. F. Martínez,[a] B. J. Ayers,[a] M. A. Hollas,[a] N. Ngo,[a] S. Nakagawa,[c] A. Kato,*[c] T. D. Butters,[b] G. W. J. Fleet[a,b] and S. F. Jenkinson*[a]

[a] *Chemistry Research Laboratory, 12 Mansfield Road, Oxford, OX1 3TA, United Kingdom. Fax: +44 (0)1865 285002; Tel: +44 (0)1865 275645; E-mail: sarah.jenkinson@chem.ox.ac.uk*
[b] *Oxford Glycobiology Institute, University of Oxford, South Parks Road, Oxford, OX1 3QU, United Kingdom. Fax: +44 (0)1865 275216; Tel: +44 (0)1865 275342.*
[c] *Department of Hospital Pharmacy, University of Toyama, 2630 Sugitani, Toyama 930-0194, Japan; E-mail: kato@med.u-toyama.ac.jp*

SUPPORTING INFORMATION

1. Computational Data

DFT calculations at the M06-2X/6-311++G**[1] level of theory using Gaussian 09[2] were performed to evaluate the optimized geometries of **10**, **13**, **11**, **38**, **12**, **21** and **42** in gas phase.

Cartesian coordinates for **10**

Standard orientation:

Center Number	Atomic Number	Atomic Type	Coordinates (Angstroms) X	Y	Z
1	6	0	-1.596839	-1.040745	0.416731
2	6	0	-1.306110	-0.651045	-1.03377
3	7	0	0.131167	-0.447495	-1.192713
4	6	0	0.718861	0.554164	-0.299717
5	6	0	0.463688	0.176130	1.169289
6	6	0	-1.030490	-0.021868	1.409432
7	8	0	-0.985817	-2.305830	0.627939
8	8	0	0.987602	1.154662	2.033448
9	8	0	-1.649891	1.248504	1.288677
10	6	0	2.211257	0.723138	-0.592715
11	8	0	2.646568	1.819878	-0.890305
12	7	0	3.020065	-0.370260	-0.547890
13	6	0	2.728344	-1.731372	-0.122665
14	6	0	-2.129648	0.555056	-1.523494
15	8	0	-3.418790	0.541662	-0.908338
16	1	0	-2.681572	-1.116165	0.543607
17	1	0	-1.579453	-1.526024	-1.629871
18	1	0	0.368824	-0.249316	-2.158895
19	1	0	0.311444	1.562847	-0.444691
20	1	0	0.969220	-0.757387	1.412581
21	1	0	-1.167521	-0.398498	2.432800
22	1	0	-1.314027	-2.672021	1.453249
23	1	0	0.457362	1.952849	1.926381
24	1	0	-2.548642	1.142102	0.953888
25	1	0	3.988017	-0.132255	-0.714493
26	1	0	3.341505	-2.416991	-0.709396
27	1	0	1.681999	-1.964645	-0.309454
28	1	0	2.957839	-1.881993	0.936869
29	1	0	-1.613344	1.485509	-1.276669
30	1	0	-2.227786	0.488137	-2.612112
31	1	0	-3.994238	1.156372	-1.369434

Cartesian coordinates for **13**

Standard orientation:

Center Number	Atomic Number	Atomic Type	Coordinates (Angstroms) X	Y	Z
1	6	0	-1.697574	0.590974	0.528928
2	6	0	-1.485356	-0.398496	-0.614038
3	7	0	-0.136880	-0.954171	-0.538875
4	6	0	0.903164	0.070506	-0.651001
5	6	0	0.766679	1.074874	0.503942
6	6	0	-0.629311	1.690141	0.487112
7	8	0	-1.612944	-0.111615	1.761458
8	8	0	1.760808	2.066889	0.441182
9	8	0	-0.719107	2.452701	-0.708441
10	6	0	2.299837	-0.550910	-0.694552
11	8	0	3.043163	-0.296820	-1.623813
12	7	0	2.673702	-1.404044	0.297604
13	6	0	2.003320	-1.726426	1.548473
14	6	0	-2.492137	-1.533960	-0.540038
15	8	0	-3.784825	-0.959575	-0.656407
16	1	0	-2.693469	1.031254	0.403863
17	1	0	-1.653655	0.158823	-1.548529
18	1	0	-0.009443	-1.639072	-1.277927
19	1	0	0.827481	0.635080	-1.591218
20	1	0	0.892115	0.565981	1.458829
21	1	0	-0.726240	2.343763	1.363976
22	1	0	-2.051012	0.402407	2.443323
23	1	0	1.611443	2.578459	-0.362160
24	1	0	-1.476949	3.040170	-0.663893
25	1	0	3.630407	-1.711906	0.191138
26	1	0	2.248289	-2.754686	1.818762
27	1	0	0.924864	-1.654706	1.421470
28	1	0	2.325625	-1.068418	2.361663
29	1	0	-2.303857	-2.238570	-1.360340
30	1	0	-2.367978	-2.053496	0.414150
31	1	0	-4.443862	-1.640438	-0.508993

Cartesian coordinates for **11**

Standard orientation:

Center Number	Atomic Number	Atomic Type	Coordinates (Angstroms) X	Y	Z
1	7	0	0.024301	0.110887	-1.217110
2	6	0	-0.599266	-0.748632	-0.209823
3	6	0	-0.007321	-0.256105	1.131268
4	6	0	1.154342	0.686076	0.745946
5	6	0	1.371275	0.425530	-0.748007
6	8	0	0.738752	2.013698	1.022803
7	8	0	0.427872	-1.400132	1.841885
8	6	0	-2.127643	-0.751836	-0.265683
9	8	0	-2.726102	-1.812410	-0.263257
10	7	0	-2.791565	0.433860	-0.294162
11	6	0	-2.275697	1.792525	-0.384521
12	6	0	2.379256	-0.705388	-0.947212
13	8	0	3.647218	-0.195450	-0.567405
14	1	0	0.009460	-0.305489	-2.141412
15	1	0	-0.325882	-1.805671	-0.299361
16	1	0	-0.739393	0.309757	1.716261
17	1	0	2.050966	0.434322	1.319981
18	1	0	1.756670	1.316992	-1.254225
19	1	0	1.432793	2.617878	0.746634
20	1	0	0.590763	-1.155457	2.756275
21	1	0	-3.790959	0.307747	-0.368447
22	1	0	-3.039742	2.465518	0.006697
23	1	0	-2.041470	2.070549	-1.414260
24	1	0	-1.373646	1.917661	0.209433
25	1	0	2.100830	-1.569780	-0.331670
26	1	0	2.377980	-1.009260	-2.001760
27	1	0	4.290887	-0.906651	-0.56925

Cartesian coordinates for **38**

Standard orientation:

Center Number	Atomic Number	Atomic Type	Coordinates (Angstroms) X	Y	Z
1	7	0	-0.088601	-0.521533	-1.092470
2	6	0	0.920533	0.457547	-0.683925
3	6	0	0.311890	1.136295	0.560457
4	6	0	-1.189767	0.779767	0.522226
5	6	0	-1.385224	0.109298	-0.849489
6	8	0	-1.462702	-0.091185	1.605094
7	8	0	0.564055	2.522407	0.448384
8	6	0	2.304058	-0.163257	-0.487705
9	8	0	3.249981	0.252058	-1.131228
10	7	0	2.446462	-1.185960	0.398377
11	6	0	1.473215	-1.766982	1.309007
12	6	0	-2.496731	-0.924608	-0.854422
13	8	0	-3.640376	-0.317017	-0.257723
14	1	0	0.040566	-0.797929	-2.059600
15	1	0	1.070454	1.249741	-1.427047
16	1	0	0.729977	0.740966	1.490912
17	1	0	-1.792204	1.688821	0.599402
18	1	0	-1.612176	0.902838	-1.578134
19	1	0	-2.410862	-0.265424	1.592568
20	1	0	0.376133	2.940956	1.292051
21	1	0	3.403674	-1.501839	0.468639
22	1	0	0.465963	-1.609198	0.933114
23	1	0	1.551397	-1.341790	2.314344
24	1	0	1.648256	-2.842204	1.372183
25	1	0	-2.167897	-1.792640	-0.274367
26	1	0	-2.714372	-1.245788	-1.878575
27	1	0	-4.409443	-0.872521	-0.399958

Cartesian coordinates for **12**

Standard orientation:

Center Number	Atomic Number	Atomic Type	Coordinates (Angstroms) X	Y	Z
1	6	0	0.469499	-0.935365	0.522990
2	6	0	1.472648	-0.599899	-0.588191
3	7	0	0.368521	0.040021	-1.341358
4	6	0	-0.618796	-0.737454	-0.563310
5	8	0	0.639077	-2.209169	1.074044
6	6	0	-1.957157	-0.132247	-0.169622
7	8	0	-2.937531	-0.859518	-0.141056
8	7	0	-2.045765	1.180630	0.168419
9	6	0	-0.986371	2.135080	0.465658
10	6	0	2.663490	0.274844	-0.273725
11	8	0	2.227605	1.380603	0.498270
12	1	0	0.439821	-0.149534	1.283917
13	1	0	1.817271	-1.538788	-1.040686
14	1	0	-0.852026	-1.712197	-1.003326
15	1	0	-0.063594	-2.376485	1.708276
16	1	0	-2.982393	1.426798	0.459556
17	1	0	-1.317767	3.130213	0.165392
18	1	0	-0.087596	1.886104	-0.089859
19	1	0	-0.751194	2.153228	1.534668
20	1	0	3.401189	-0.321110	0.278033
21	1	0	3.117604	0.609920	-1.214943
22	1	0	2.970705	1.966277	0.654567
23	1	0	0.355596	-0.144074	-2.337889

Cartesian coordinates for **21**

Standard orientation:

Center Number	Atomic Number	Atomic Type	Coordinates (Angstroms) X	Y	Z
1	7	0	-0.252196	0.366084	1.416536
2	6	0	0.298822	-0.657521	0.526936
3	6	0	-0.697543	-0.713969	-0.655827
4	6	0	-1.939015	0.060828	-0.159226
5	6	0	-1.700561	0.182215	1.343949
6	8	0	-1.942468	1.316342	-0.820970
7	8	0	-0.969364	-2.076330	-0.911830
8	6	0	1.753399	-0.420045	0.127725
9	8	0	2.566417	-1.318151	0.248473
10	7	0	2.106974	0.789334	-0.384168
11	6	0	1.329802	2.014185	-0.506737
12	1	0	0.104895	0.266132	2.359726
13	1	0	0.289733	-1.659803	0.973148
14	1	0	-0.305123	-0.218369	-1.549202
15	1	0	-2.849743	-0.500266	-0.390473
16	1	0	-2.232946	1.024110	1.794221
17	1	0	-2.598293	1.886213	-0.411589
18	1	0	-1.354042	-2.160176	-1.787634
19	1	0	3.096780	0.844403	-0.578531
20	1	0	1.759509	2.604388	-1.317348
21	1	0	1.347759	2.600553	0.414852
22	1	0	0.290810	1.803494	-0.746693
23	1	0	-2.038892	-0.747649	1.826643

Cartesian coordinates for **42**

Standard orientation:

Center Number	Atomic Number	Atomic Type	Coordinates (Angstroms) X	Y	Z
1	6	0	-0.483082	-0.169017	-0.739255
2	6	0	-1.225485	0.769951	0.248865
3	7	0	-0.070587	0.672156	1.164907
4	6	0	0.441229	-0.519911	0.448114
5	8	0	-1.180009	-1.268735	-1.250888
6	6	0	1.947754	-0.640712	0.253682
7	8	0	2.499764	-1.697606	0.497915
8	7	0	2.656193	0.436335	-0.186149
9	6	0	2.182593	1.721741	-0.671157
10	6	0	-2.514662	0.165224	0.768525
11	8	0	-3.435345	0.201024	-0.317150
12	1	0	0.026588	0.384914	-1.532130
13	1	0	-1.422757	1.784765	-0.108924
14	1	0	0.122517	-1.473181	0.877107
15	1	0	-2.050811	-0.962771	-1.530299
16	1	0	3.634185	0.219263	-0.318427
17	1	0	2.949643	2.471663	-0.474640
18	1	0	1.284788	2.010843	-0.130273
19	1	0	1.983737	1.708032	-1.747479
20	1	0	-2.339032	-0.865967	1.096758
21	1	0	-2.884962	0.753697	1.616279
22	1	0	-4.280260	-0.157330	-0.035783
23	1	0	-0.288243	0.525507	2.144849

2. Biological Data - Glycosidase Inhibition

Table 1: Concentration of iminosugars with 2*S*, 3*R* configuration giving 50 % inhibition of various glycosidases

	IC_{50} (μM)				
	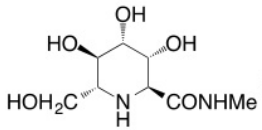	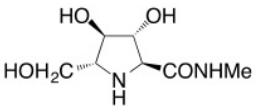	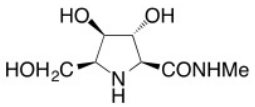	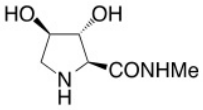	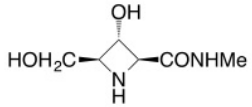
Enzyme	**10**	**11**	**38**	**21**	**12**
α-Glucosidase					
Yeast	NI[a] (35.8%)	NI[a] (47.2%)	NI[a] (7.4%)	721	NI[a] (23.2%)
β-Glucosidase					
Bovine liver	NI[a] (13.8%)	NI[a] (12.0%)	NI[a] (7.6%)	NI[a] (0.5%)	NI[a] (6.2%)
α-Galactosidase					
Coffee beans	NI[a] (36.2%)	NI[a] (1.4%)	NI[a] (0%)	NI[a] (6.0%)	NI[a] (2.3%)
β-Galactosidase					
Bovine liver	NI[a] (40.3%)	NI[a] (22.4%)	NI[a] (1.9%)	NI[a] (0%)	NI[a] (3.2%)
α-Mannosidase					
Jack bean	NI[a] (19.3%)	NI[a] (4.5%)	NI[a] (0%)	NI[a] (0%)	NI[a] (0%)
β-Mannosidase					
Snail	NI[a] (2.0%)	NI[a] (10.8%)	NI[a] (1.3%)	NI[a] (0%)	NI[a] (0.7%)
α-L-Rhamnosidase					
Penicillium decumbens	NI[a] (0.1%)	NI[a] (12.8%)	NI[a] (0.5%)	NI[a] (7.7%)	NI[a] (0.2%)
α-L-Fucosidase					
Bovine kidney	NI[a] (6.3%)	NI[a] (0%)	NI[a] (11.0%)	NI[a] (1.2%)	NI[a] (0%)

NI[a] : No inhibition (less than 50% inhibition at 1000 μM) ; ( ): inhibition % at 1000 μM.

NI[b] : No inhibition (less than 50% inhibition at 500 μM) ; ( ): inhibition % at 500 μM.

[ ][c] : Data from Shilvock et al., 1998. [5]

Table 2: Concentration of enantiomeric (**31**, **39**, **40**, **41**) and epimeric (**13**) iminosugars giving 50 % inhibition of various glycosidases

	IC_{50} (μM)				
	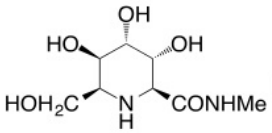	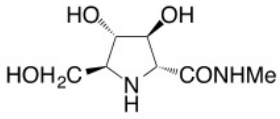	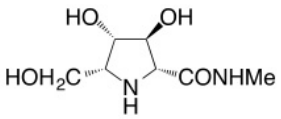	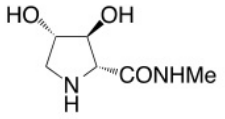	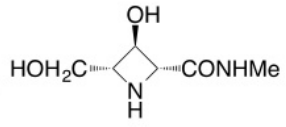
Enzyme	**13**	**39**	**40**	**31**	**41**
α-Glucosidase					
Yeast	NI[a] (14.1%)	NI[a] (9.3%)	NI[a] (11.2%)	NI[a] (3.9%)	NI[a] (31.3%)
β-Glucosidase					
Bovine liver	NI[a] (22.1%)	NI[a] (0%)	NI[a] (2.2%)	NI[a] (2.2%)	NI[a] (9.9%)
α-Galactosidase					
Coffee beans	NI[a] (11.7%)	NI[a] (9.6%)	NI[a] (32.9%)	NI[a] (10.4%)	332
β-Galactosidase					
Bovine liver	NI[a] (2.7%)	NI[a] (1.1%)	NI[a] (2.9%)	NI[a] (0.1%)	NI[a] (33.4%)
α-Mannosidase					
Jack bean	NI[a] (0%)	NI[a] (0%)	NI[a] (3.2%)	NI[a] (0.7%)	NI[a] (0%)
β-Mannosidase					
Snail	NI[a] (0%)	NI[a] (1.6%)	NI[a] (0.4%)	NI[a] (0%)	NI[a] (0%)
α-L-Rhamnosidase					
Penicillium decumbens	NI[a] (1.2%)	NI[a] (1.9%)	NI[a] (0%)	NI[a] (0%)	NI[a] (0.3%)
α-L-Fucosidase					
Bovine kidney	NI[a] (2.3%)	NI[a] (0%)	NI[a] (1.2%)	NI[a] (5.4%)	NI[a] (4.5%)

NI[a] : No inhibition (less than 50% inhibition at 1000 μM) ; ( ): inhibition % at 1000 μM.

NI[b] : No inhibition (less than 50% inhibition at 500 μM) ; ( ): inhibition % at 500 μM.

Table 3. Concentration of pyrrolidine amide 11 and derivatives giving 50 % inhibition of various glycosidases

	IC_{50} (μM)			
	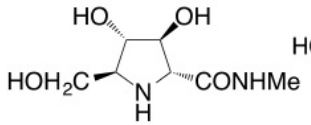	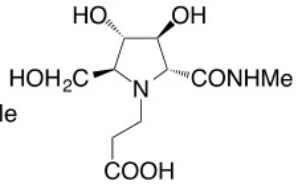	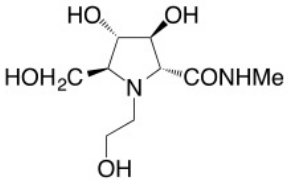	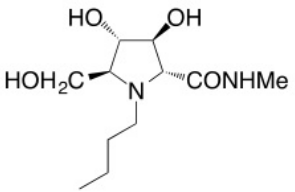
Enzyme	**11**	**37**	**36**	**35**
α-Glucosidase				
Yeast	NI[a] (47.2%)	NI[a] (5.5%)	NI[a] (24.3%)	NI[a] (10.3%)
β-Glucosidase				
Bovine liver	NI[a] (12.0%)	NI[a] (2.4%)	NI[a] (12.9%)	NI[a] (3.0%)
α-Galactosidase				
Coffee beans	NI[a] (1.4%)	745	NI[a] (0%)	NI[a] (0%)
β-Galactosidase				
Bovine liver	NI[a] (22.4%)	NI[a] (5.2%)	NI[a] (29.3%)	NI[a] (4.2%)
α-Mannosidase				
Jack bean	NI[a] (4.5%)	NI[a] (0%)	NI[a] (0%)	NI[a] (0%)
β-Mannosidase				
Snail	NI[a] (10.8%)	NI[a] (0%)	NI[a] (0%)	NI[a] (0.7%)
α-L-Rhamnosidase				
Penicillium decumbens	NI[a] (12.8%)	NI[a] (0.5%)	NI[a] (0%)	NI[a] (1.7%)
α-L-Fucosidase				
Bovine kidney	NI[a] (0%)	NI[a] (0%)	NI[a] (2.6%)	NI[a] (0%)

NI[a] : No inhibition (less than 50% inhibition at 1000 μM) ; ( ): inhibition % at 1000 μM.

Concentration of iminosugars giving 50 % inhibition of various glycosidases

	IC_{50} (μM)	
	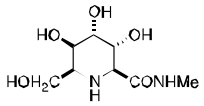	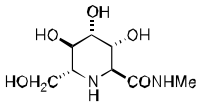
Enzyme	**13**	**10**
α-Glucosidase		
Yeast	NI (14.1%)[§]	NI (35.8%)
β-Glucosidase		
Almond	NI (9.0%)	NI (7.2%)
Bovine liver	NI (22.1%)	NI (13.8%)
α-Galactosidase		
Coffee beans	NI (11.7%)	NI (36.2%)
Human Lysosome	NI (0.5%)	NI (0%)
β-Galactosidase		
Bovine liver	NI (2.7%)	NI (40.3%)
α-Mannosidase		
Jack beans	NI (0%)	NI (19.3%)
β-Mannosidase		
Snail	NI (0%)	NI (2.0%)
α-L-Rhamnosidase		
P. decumbens	NI (1.2%)	NI (0.1%)
α-L-Fucosidase		
Bovine epididymis	NI (2.3%)	NI (6.3%)

Not determined; § No inhibition at 1000 μM (% inhibition).

Concentration of iminosugars giving 50 % inhibition of various glycosidases

	IC_{50} (μM)	
	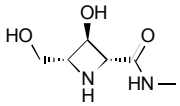	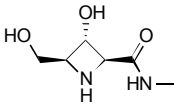
Enzyme	**41**	**12**
α-Glucosidase		
Rice	ND[#]	NI[§] (0%)
Yeast	ND	NI (23.2%)
Aspergillus niger	ND	NI (7.8%)
β-Glucuronidase		
E. coli	**59**	NI (22.8%)
Bovine liver	NI (12.1%)	NI (0%)
α,α-Trehalase		
Porcine kidney	ND	NI (3.0%)
Amyloglucosidase		
Aspergillus niger	ND	NI (0%)
Rhizopus sp.	ND	NI (0%)

Not determined; § No inhibition at 1000 μM (% inhibition).

3. Reliability of molecular modelling for azetidine structures

Molecular modeling has been used to successfully calculate structures and molecular shapes for iminosugars. For example DFT calculations were used to predict the structure of strained azetidine shown in Figure 3.1, which was found to compare very favorably to the structure obtained using X-ray crystallography.[3] The overlap of the two structures shows that molecular modeling is a reliable method for estimating the conformation of iminosugars generally and of azetidines specifically (Figure 3.1).

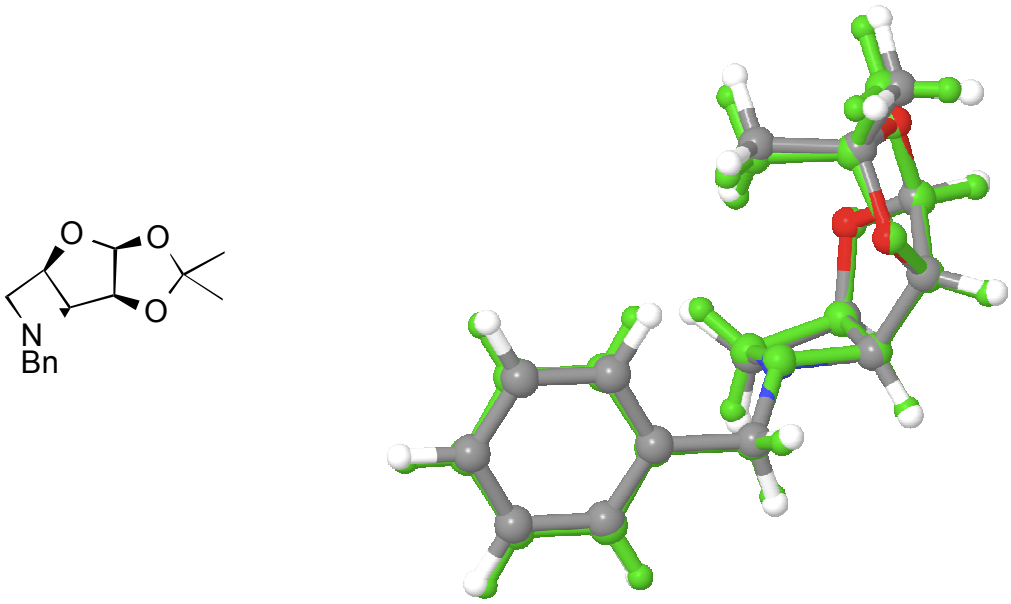

Figure 3.1: Overlay of structure obtained by X-ray analysis with structure obtained from molecular modelling showing the validity of the modeling for aztidine compounds

4. Free oligosaccharide (FOS) analysis overview and results in GU units

Five Stages of FOS Analysis[4]

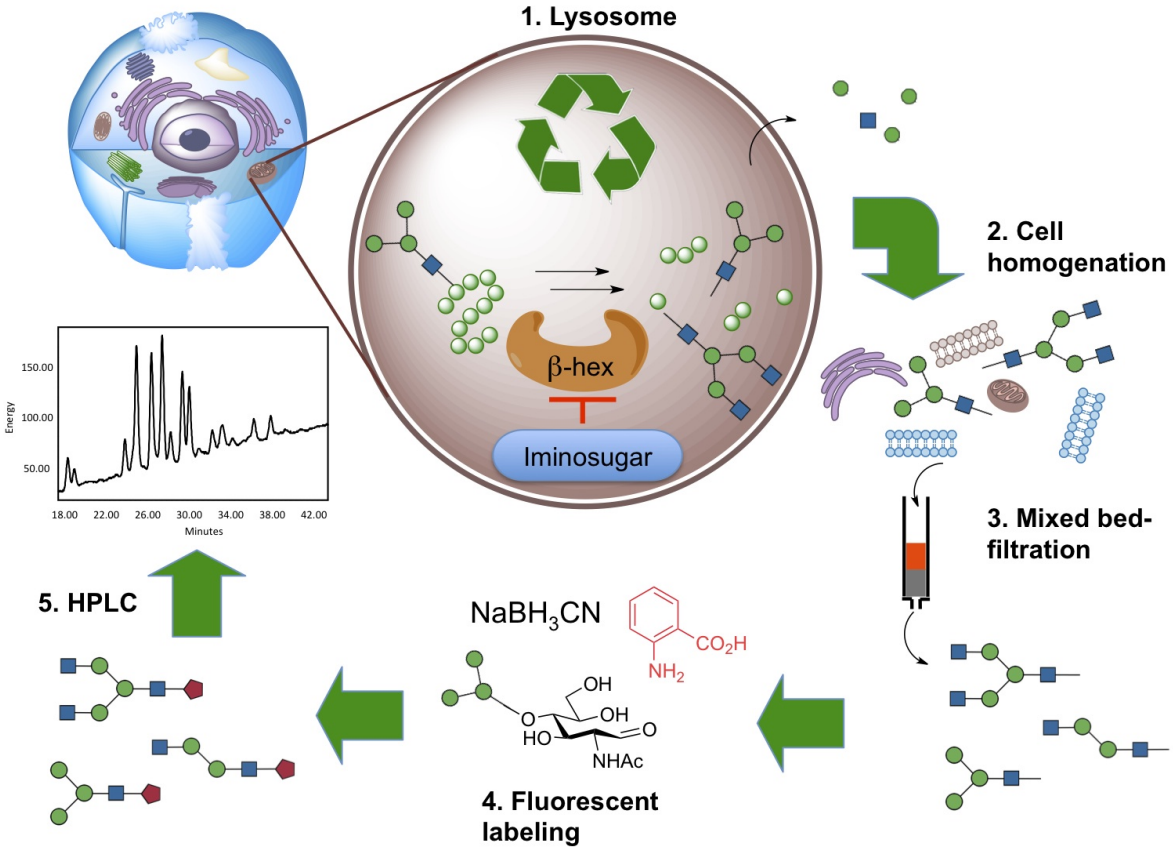

Figure 4.1: 1) Cells are grown in presence of iminosugar causing incomplete breakdown of oligosaccharides and resulting in accumulation of species with additional terminal carbohydrate residues; 2) Cells are homogenized to liberate oligosaccharides from cells and organelles; 3) Oligosaccharides are purified by removal of cellular debris; 4.) Using reductive amination the reducing terminus of the oligosaccharide is fluorescently labelled with 2-AA; 5) HPLC anaylsis in comparison to reference to identify oligosaccharides present.

FOS analysis results in GU units

Structures, retention time in glucose units (GUs) and relative intensity in percent of FOS peaks isolated from a control experiment and 200 μM D-manno amide **11** treated HL60 cells. Peak IDs labeled according to Figure 4.24. Intensity measurements are the mean value of three independent measurements (±S.D.). The species were assigned according literature values.[4] Labels are as follows: ◇ Glucose; ● Mannose; ⬟ 2-Aminobenzoic acid; ■ *N*-Acetyl-glucosamine; ∗ Proposed structure.

ID	Untreated GU	Treated GU	Structure name	Structure	Untreated cells [%]	Treated cells [%]
1	-	3.71	$GlcNAc_1Man_2GlcNAc_1$	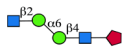	-	3.88 ± 0.06
2	-	3.83	$GlcNAc_2Man_2GlcNAc_1$	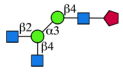	-	2.62 ± 0.18
3	4.16	4.10	$Man_3GlcNAc_1$		2.06 ± 0.25	1.12 ± 0.41
4	4.94	4.92	$Man_4GlcNAc_1$	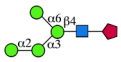	13.43 ± 0.15	4.40 ± 0.16
5	-	**5.19**	$GlcNAc_2Man_3GlcNAc_1$	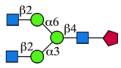	-	**15.85 ± 0.43**
6	-	5.57	$GlcNAc_3Man_3GlcNAc_1$	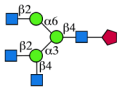	-	13.55 ± 0.26
6A	5.67	-	$Man_5GlcNAc_1$	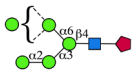	4.16 ± 0.82	-
7	**5.86**	**5.84**	$Man_5GlcNAc_1$	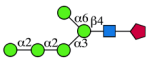	**36.28 ± 1.20**	**15.67 ± 0.39**
8	-	6.06	$GlcNAc_4Man_3GlcNAc_1$	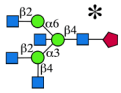	-	4.18 ± 0.00
9	-	6.39	$GlcNAc_4Man_3GlcNAc_1$	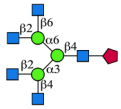	-	11.09 ± 0.24
10	6.60	6.59	$Glc_1Man_5GlcNAc_1$	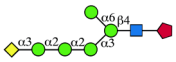	19.48 ± 0.89	8.43 ± 0.12
11	-	6.86	$GlcNAc_5Man_3GlcNAc_1$	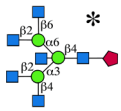	-	1.65 ± 0.15
12	7.29	7.29	$Glc_2Man_5GlcNAc_1$	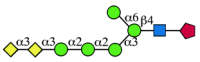	6.25 ± 0.20	3.20 ± 0.22
13	-	7.60	$GlcNAc_5Man_3GlcNAc_1$	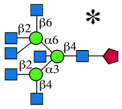	-	4.53 ± 0.16
14	7.97	7.95	$Man_7GlcNAc_2$	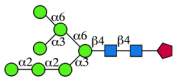	3.94 ± 0.23	1.86 ± 0.12
15	8.42	8.31	$Man_8GlcNAc_2$	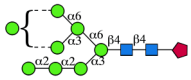	1.52 ± 0.66	0.83 ± 0.09
16	8.75	8.74	$Man_8GlcNAc_2$	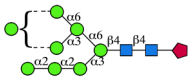	5.61 ± 0.21	4.12 ± 0.13
17	9.43	9.42	$Man_9GlcNAc_2$	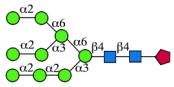	7.27 ± 0.16	3.01 ± 0.06

5. Cancer invasion overview and cytotoxicity measurement of pyrrolidine iminosugars

Stages of cancer invasion

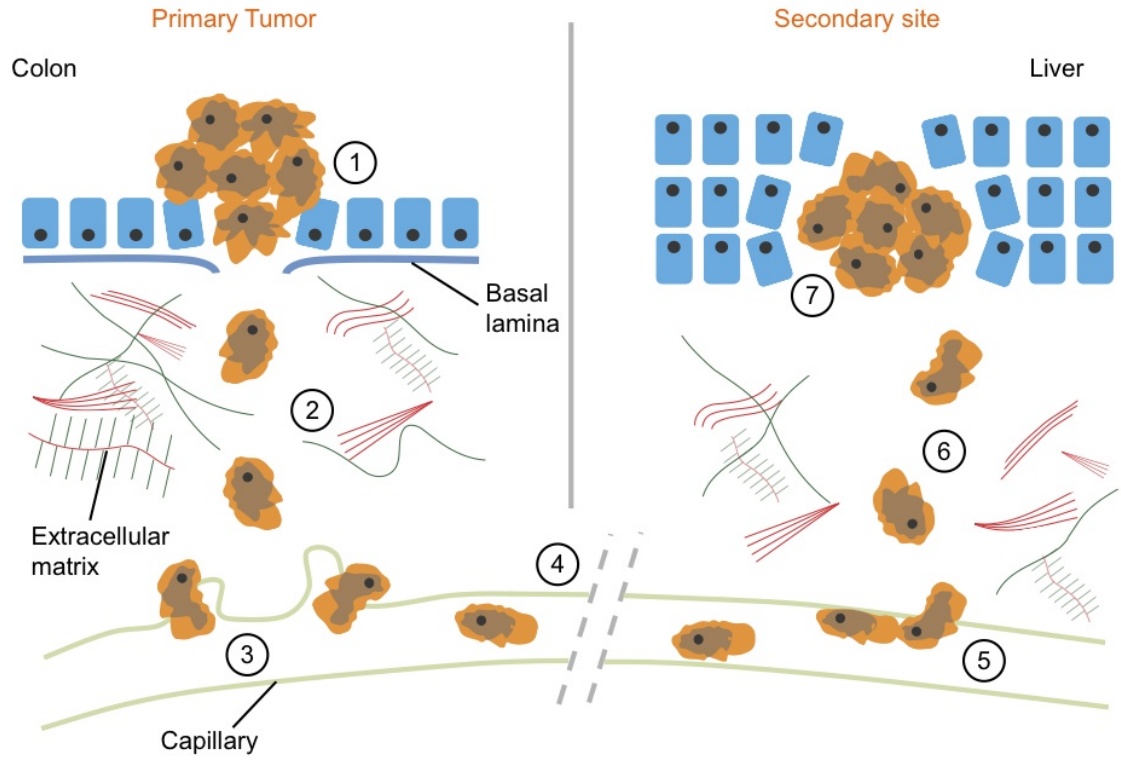

Figure 5.1: Example of colorectal cancer metastasis to the liver: 1) cancer cell shedding by primary tumour; 2) local invasion of the ECM and breaking through the basal lamina; 3) intravasation, entering the blood vessel assisted by leaky vessels due to stimulated angiogenesis; 4) cancer cells travel through the blood stream, less than 1 in 1000 cells are successful; 5) blood vessel adhesion and extravasation; 6) local invasion of secondary site; 7) micrometastasis formation, which grows into secondary tumour.

Boyden chamber setup

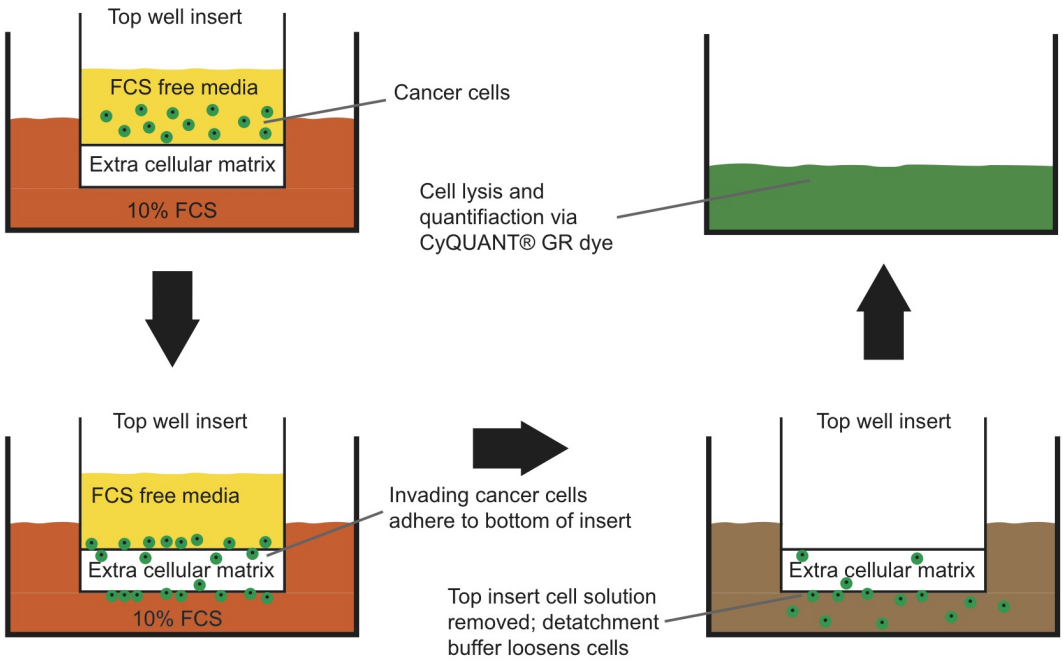

Figure 5.2: 1) MDA-MB-231 cells starved for 24 h in fetal calf serum free media, were seeded on top of an insert connected via pores blocked with reconstituted basement membrane matrix to a well containing 10% FCS as chemoattractant. 2) During an incubation time of 64 h the cells were allowed to invade through the basement membrane and adhere to the bottom of the insert. 3) Following completion of the assay the cells were detached from the bottom of the insert. 4) The cells were lysed and fluorescence was used to quantify of the number of invaded cells.

Cytotoxicity measurement of pyrrolidine iminosugars

To ensure that the observed trends were not due to protein variations in the collected samples a bicinchoninic acid (BCA) assay was performed indicating stable protein levels within error of the technique. Furthermore to rule out cytotoxicity of the iminosugars as a confounding factor their influence on cell proliferation was tested in an assay involving 3-(4,5-dimethylthiazol-2-yl)-5-(3-carboxymethoxyphenyl)-2-(4-sulfophenyl)-2H-tetrazolium (MTS). The assay was performed at the same concentrations used for the FOS assay both at a one and three day timepoint, but none of the iminosugar derivatives **11**, **35-37** displayed any cytotoxicity even at the highest concentration of 200 μM (Figure 5.3).

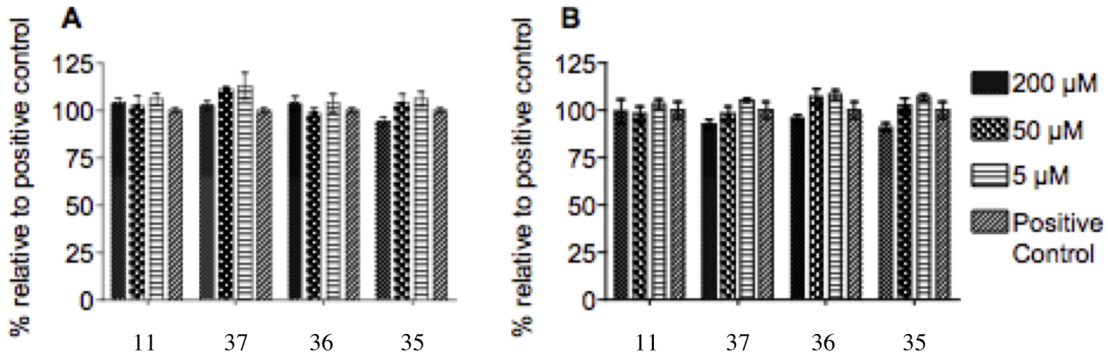

Figure 5.3: HL60 cell proliferation evaluated using an MTS assay in presence of D-manno pyrrolidine **11** and derivatives relative to untreated control (H_2O instead of inhibitor) with 12500 cells/well. A) 24 h reading; B) 72 h reading.

To equally rule out toxicity of the investigated iminosugars **11** the cell line used in the cell invasion assay was probed with an MTS assay. Therefore MDA-MB-231 cells were incubated for 24 h and 72 h with the iminosugars at range of concentrations from 5 μM to 1 mM and their ability to metabolize MTS was investigated. Even at the highest concentration employed no cytotoxicity was detectable for the iminosugars **11** for any of the time points.

6. Lineweaver Burk plots for pyrrolidines

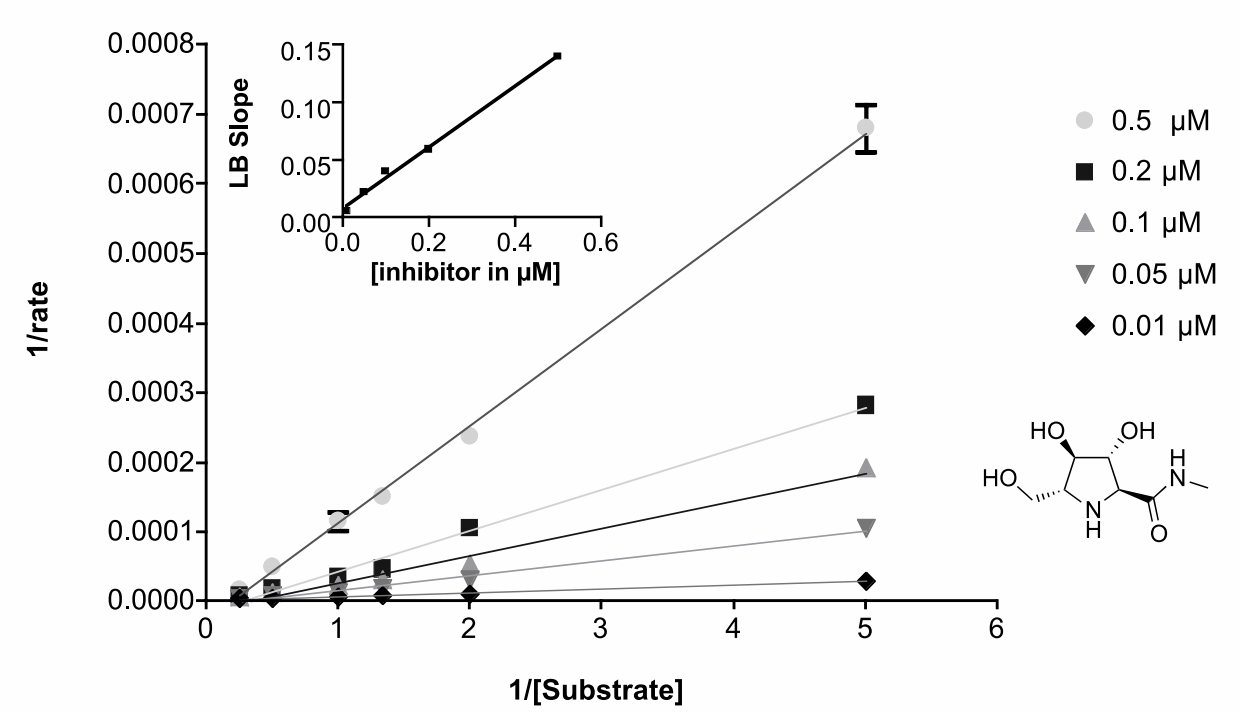

Figure 6.1 Lineweaver Burk (LB) plot of pyrrolidine amide 11 against β-*N*-acetylglucosaminidase derived from HL60 cell homogenate; K_i = 27 nM based on X-intercept of insert graph (LB slope vs Inhibitor concentration, R^2= 0.9946).

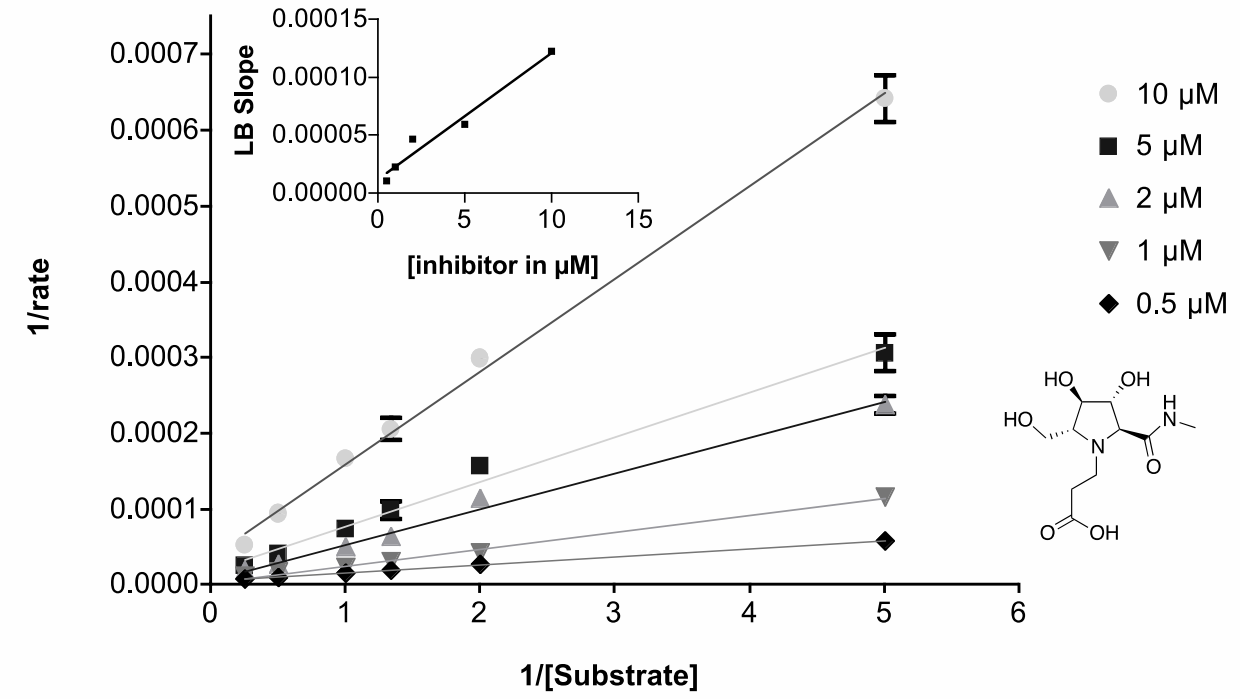

Figure 6.2 Lineweaver Burk (LB) plot of *N*-EtCOOH pyrrolidine 37 against β-*N*-acetyl-hexosaminidase derived from HL60 cell homogenate; K_i = 1.08 μM based on X-intercept of insert graph (LB slope vs Inhibitor concentration, R^2 = 0.9637).

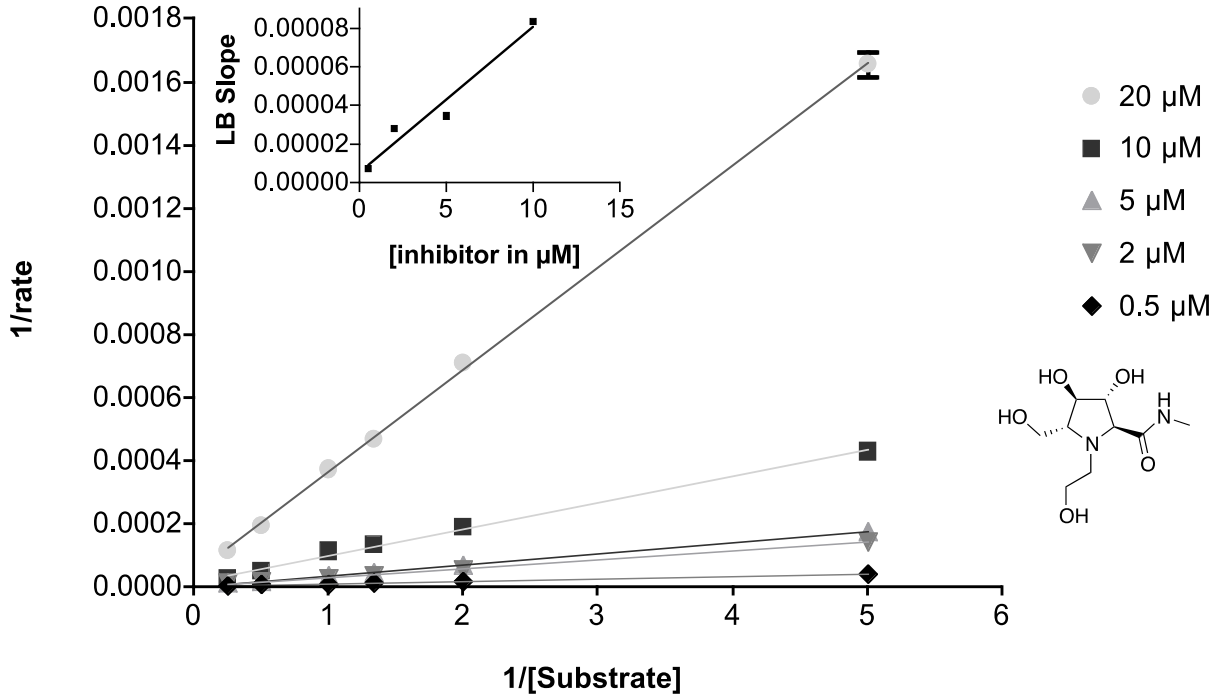

Figure 6.3 Lineweaver Burk (LB) plot of *N*-EtOH pyrrolidine 36 against β-*N*-acetyl-hexosaminidase derived from HL60 cell homogenate; K_i = 0.718 μM based on X-intercept of insert graph (LB slope vs Inhibitor concentration, R^2 = 0.9541).

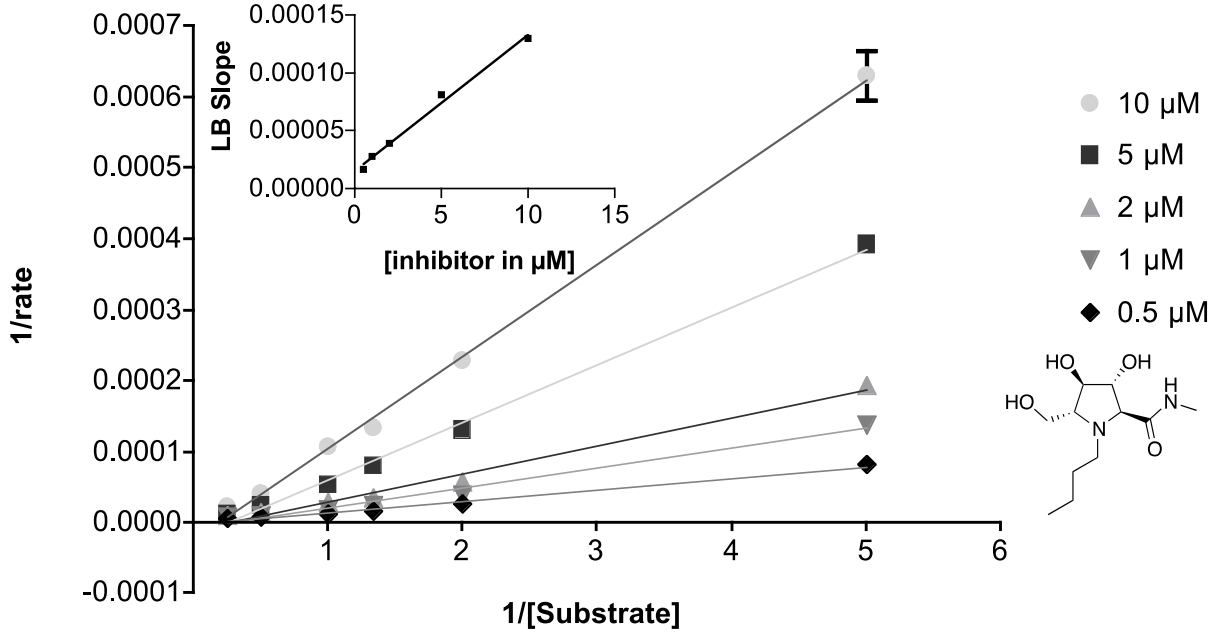

Figure 6.4 Lineweaver Burk (LB) plot of *N*-Bu pyrrolidine 35 against β-*N*-acetyl-hexosaminidase derived from HL60 cell homogenate; K_i = 1.31 μM based on X-intercept of insert graph (LB slope vs Inhibitor concentration, R^2 = 0.9898).

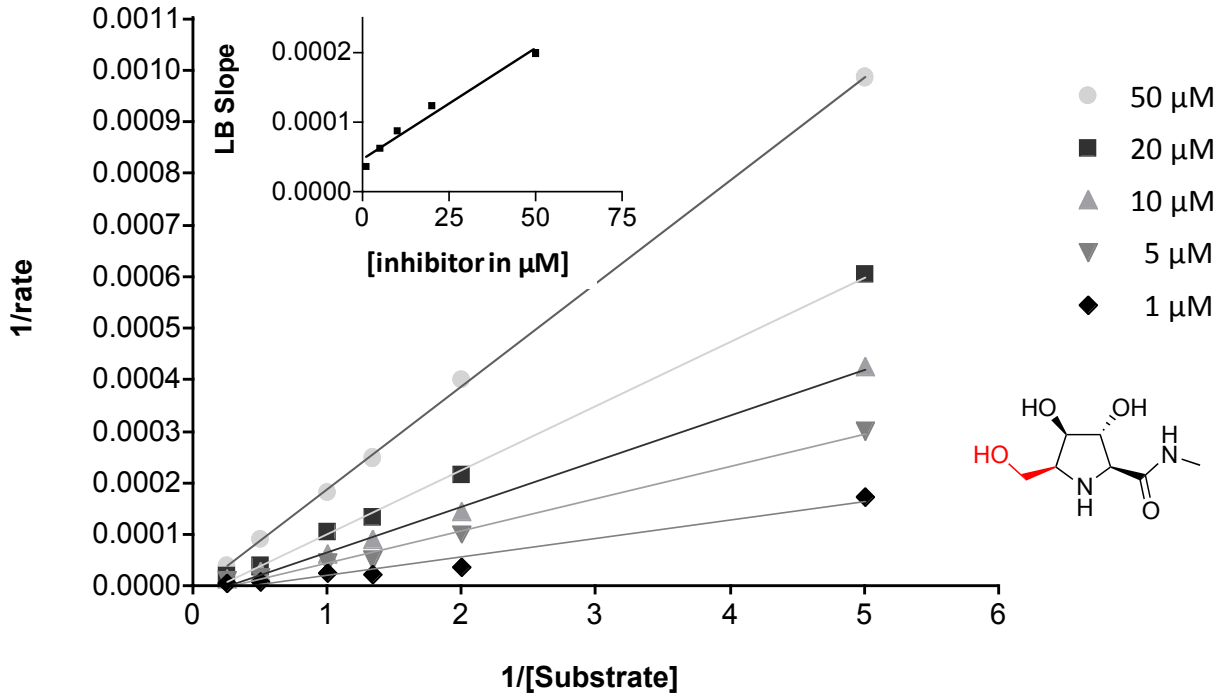

Figure 6.5 Lineweaver Burk (LB) plot of pyrrolidine amide 38 against β-*N*-acetylglucosaminidase derived from HL60 cell homogenate; K_i = 14.9 µM based on X-intercept of insert graph (LB slope vs Inhibitor concentration, R^2= 0.9683).

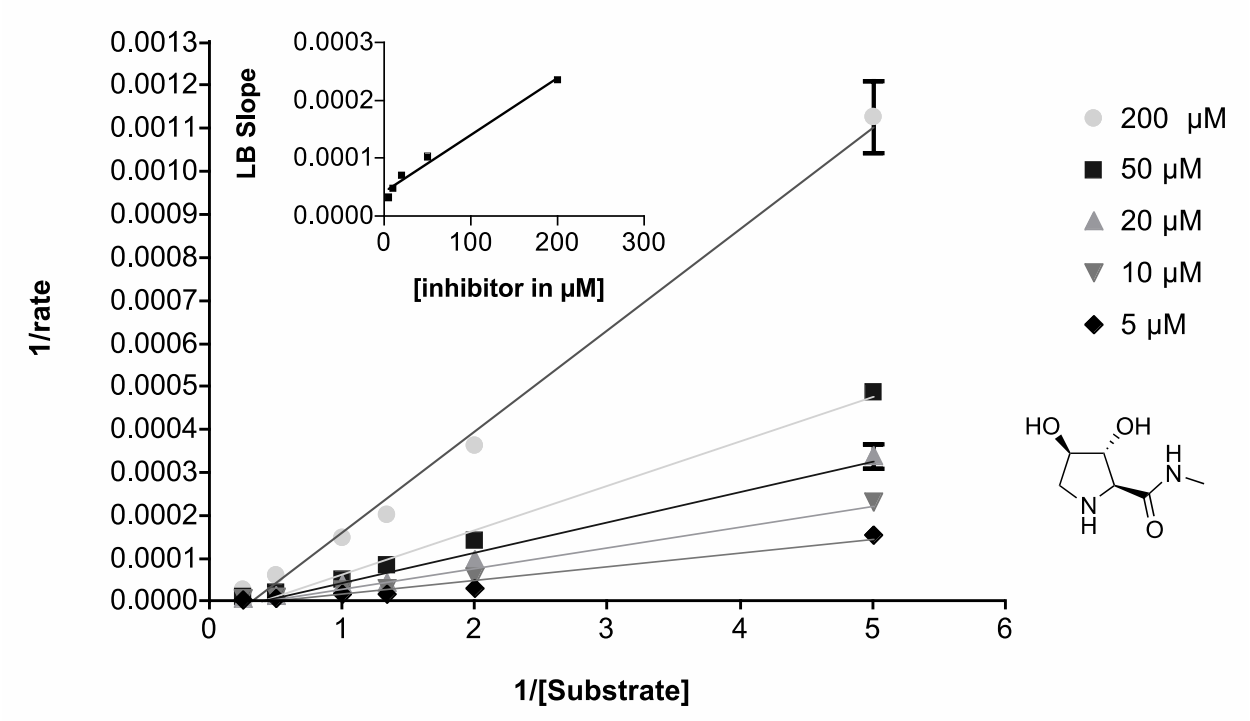

Figure 6.6 Lineweaver Burk (LB) plot of pyrrolidine amide 21 against β-*N*-acetylglucosaminidase derived from HL60 cell homogenate; K_i = 42.5 µM based on X-intercept of insert graph (LB slope vs Inhibitor concentration, R^2= 0.9825).

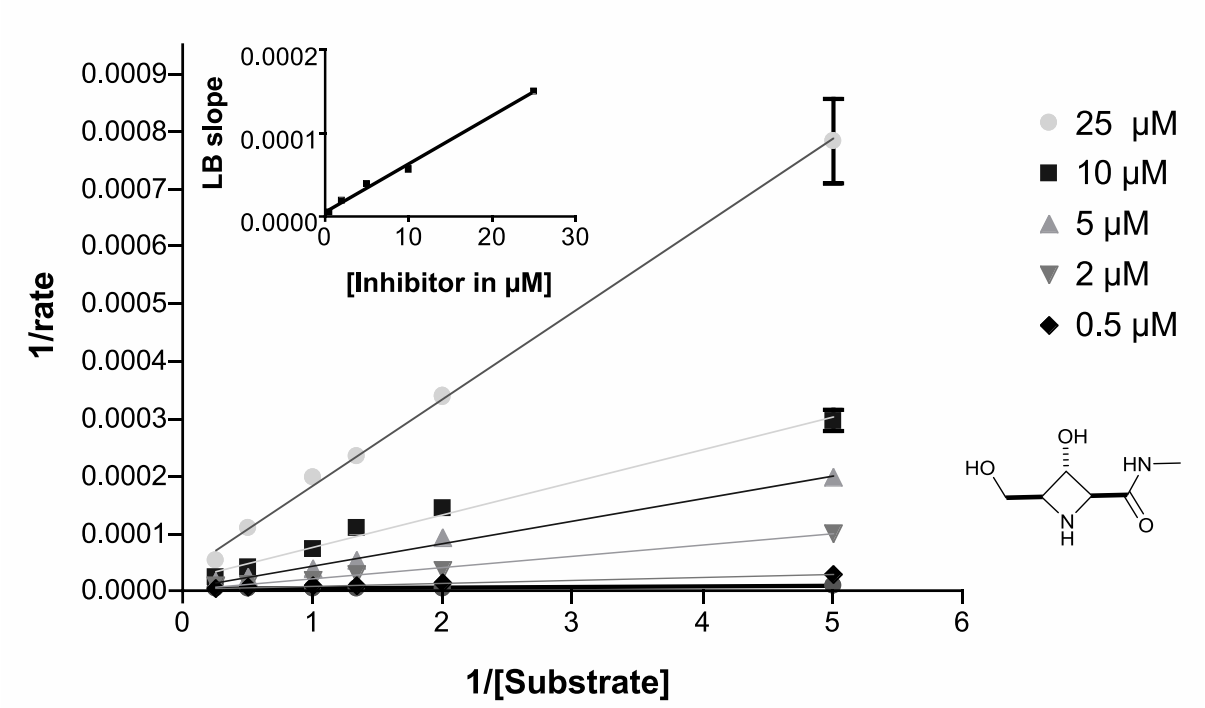

Figure 6.7 Lineweaver Burk (LB) plot of azetidine amide 12 against β-*N*-acetylglucosaminidase derived from HL60 cell homogenate; K_i = 0.892 µM based on X-intercept of insert graph (LB slope vs Inhibitor concentration, R^2= 0.9940)

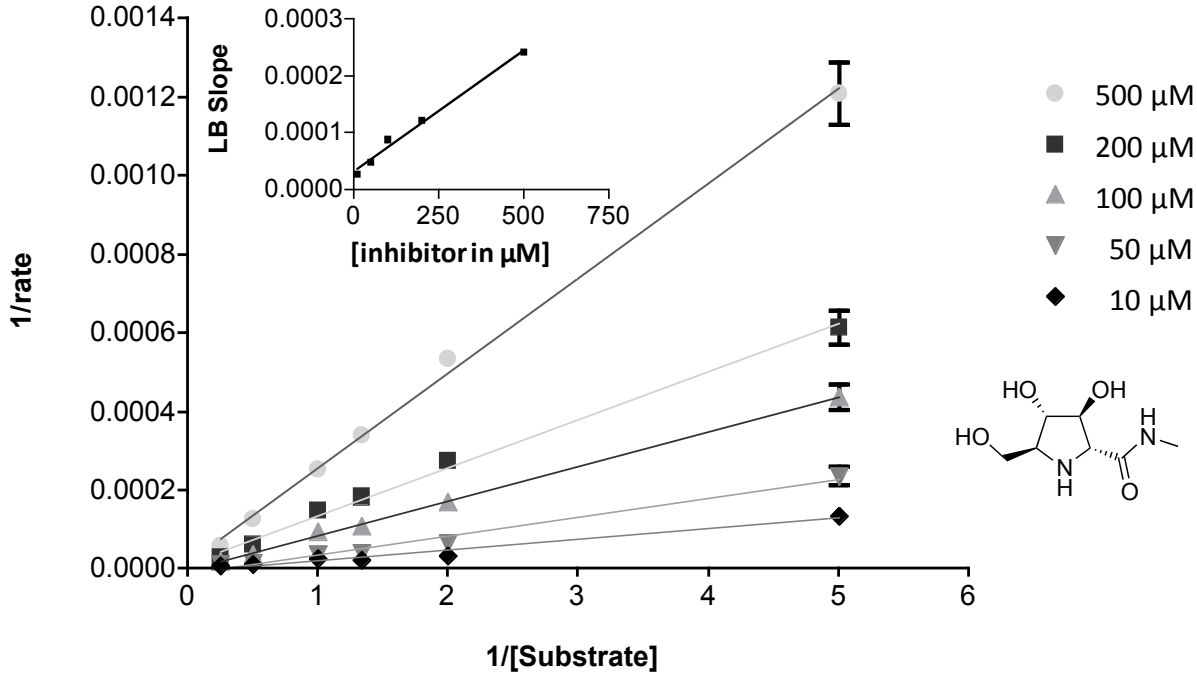

Figure 6.8 Lineweaver Burk (LB) plot of pyrrolidine amide 39 against β-*N*-acetylglucosaminidase derived from HL60 cell homogenate; K_i = 75.1 µM based on X-intercept of insert graph (LB slope vs Inhibitor concentration, R^2= 0.9887).

N.B. The data collected for Figures 6.1 – 6.8 was collected using cellular homogenate of HL-60 cells and should not be regarded as data derived from purified enzyme.

7. Additional Experimental

Experimental for piperidine amides

Pipecolic amide has been previously synthesised[5] however a modified sequence was used for the re-synthesis in this study, which as been detailed in scheme 7.1 below. The experimental detail is given from novel compound S3 onwards.

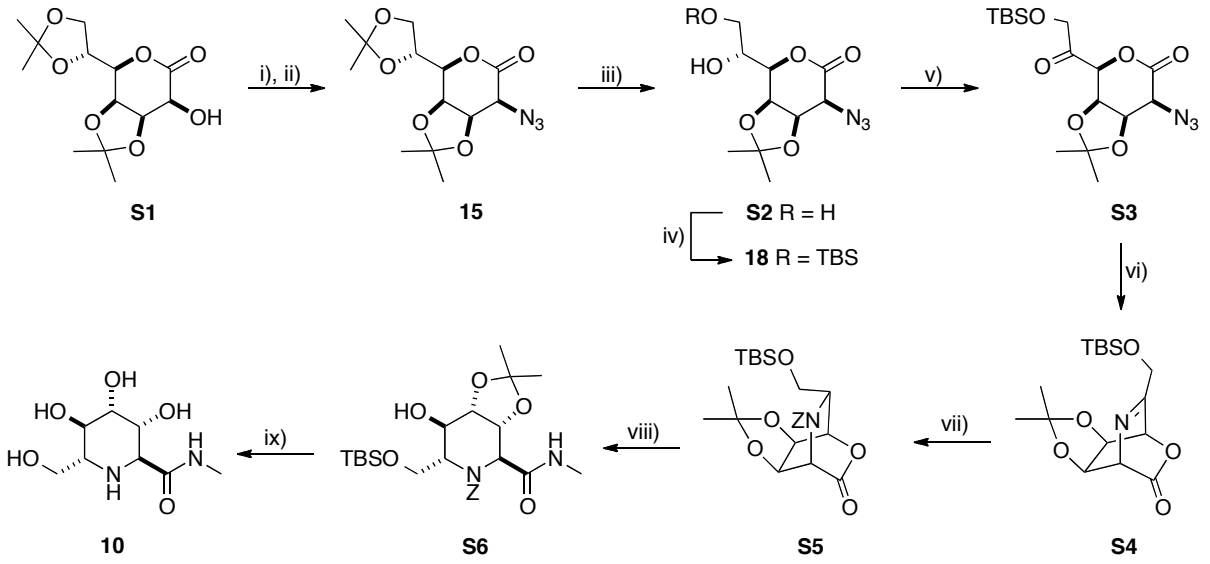

Scheme 7.1 Synthetic sequence to pipecolic amide **10**. Reagents and conditions: i) Tf_2O, Pyridine, DCM, -30 °C to -10 °C, 40 min; ii) NaN_3, DMF, 18 h, 94% over two steps; iii) aq. AcOH, 2.5 h, quant; iv) $Me_2{}^tBuSiCl$, imidazole, DMF, RT, 18 h, 92%; v) PCC, 3Å sieves, DCM, 18 h, 86% vi) $(EtO)_3P$, THF, 18 h, quant; vii) $(Ph_3P)_2CuBH_4$, CbzCl, $HCCl_3$, 5 h, 90%; viii) $MeNH_2$, THF, 18 h, 59%; ix) MeOH/HCl then Pd/C and H_2, 22 h, 95%.

2-Azido-7-*O-tert*-butyldimethylsilyl-2-deoxy-3,4-*O*-isopropylidene-D-*talo*-6-heptulosono-1,5-lactone S3

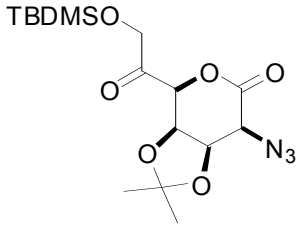

Pyridinium chlorochromate (416 mg, 1.94 mmol) was added to a flame dried flask containing powdered 3 Å molecular sieves (250 mg) along with azido-alcohol **18** (250 mg, 0.65 mmol) and dichloromethane (7 mL) was added. The reaction was stirred for 18 h at rt and the disappearance of the starting material (R_f 0.27) could be observed by t.l.c. analysis (3:1,

cyclohexane/ethyl acetate) along with formation of a new species (R_f 0.37). On completion the product was purified *via* a celite topped silica flash column (4:1, cyclohexane/ethyl acetate) to give the ketone **S3** as a white crystalline solid (215 mg, 0.56 mmol, 86%); HRMS (ESI +ve): found 408.1558 ($[M+Na]^+$); $C_{16}H_{27}N_3NaO_6Si$ requires 408.1561; m.p. 130-132 °C, [lit.[6] m.p. 120-122 °C (ether)]; $[\alpha]_D^{25}$ +4.9 (*c* 1.00, $CHCl_3$), [lit.[5] $[\alpha]_D^{20}$ +5.4 (*c* 1.00, $CHCl_3$)]; ν_{max} (thin film): 2119 (s, N_3), 1771 (s, OC=O), 1744 (s, C=O); δ_H (400 MHz, $CDCl_3$): 0.08 (3H, s, $SiCH_3$), 0.10 (3H, s, $SiCH_3$), 0.91 (9H, s, $SiC(CH_3)_3$), 1.33 (3H, s, CH_3), 1.46 (3H, s, CH_3), 3.83 (1H, d, H2, $J_{2,3}$ 3.0), 4.61 (1H, d, H7, $J_{7,7'}$ 19.9), 4.71 (2H, m, H7', H5), 4.75-4.72 (1H, m, H5), 4.87 (1H, dd, H3, $J_{3,2}$ 3.0, $J_{3,4}$ 7.7), 4.90 (1H, dd, H4, $J_{4,5}$ 1.5, $J_{4,3}$ 7.7); δ_C (100.6 MHz, $CDCl_3$): -5.4, -5.2 ($SiCH_3$), 18.6 ($SiC(\underline{C}H_3)_3$), 24.3 ($C(\underline{C}H_3)_2$), 25.8 ($C(\underline{C}H_3)_2$), 25.9 ($Si\underline{C}(CH_3)_3$), 59.6 (C2), 69.0 (C7), 75.3, 74.3 (C3, C4), 80.3 (C5), 111.9 ($\underline{C}(CH_3)_2$), 165.2 (C1), 201.7 (C6); *m/z* (ESI +ve): 825 ($[2M+Na+MeOH]^+$, 100%), 793 ($[2M+Na]^+$, 100%).

7-*O*-*tert*-Butyldimethylsilyl-2,6-deoxy-2,6-imino-3,4-*O*-isopropylidene-D-*talo*-6-heptulosono-1,5-lactone S4

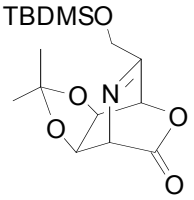

To a solution of the ketone **S3** (400 mg, 1.04 mmol) in dry tetrahydrofuran (3.3 mL) was added triethylphosphite (0.33 mL, 2.08 mmol). The reaction was left to stir at rt for 18 h and the reaction progress was monitored by t.l.c. (3:1, cyclohexane/ethyl acetate, starting material R_f 0.37, product R_f 0.46). On completion the solvent was removed *in vacuo* and the residue was purified *via* flash column chromatography (5:1, cyclohexane/ethyl acetate) and imine **S4** was isolated as a clear oil (374 mg, 1.09 mmol, quant.); HRMS (ESI +ve): found 364.1547

([M+Na]$^+$); $C_{16}H_{27}N_1NaO_5Si$ requires 364.1551; $[\alpha]_D^{25}$ +106.6 (*c* 0.99 in $CHCl_3$); [lit.[5] $[\alpha]_D^{20}$ +98.3 (*c* 1.00 in $CHCl_3$)]; ν_{max} (thin film): 1781 (s, OC=O), 1650 (w, N=C); δ_H (400 MHz, $CDCl_3$): 0.10 (6H, a-d, $Si(CH_3)_2$, *J* 9.4), 0.92 (9H, s, $SiC(CH_3)_3$), 1.31 (3H, s, CH_3), 1.33 (3H, s, CH_3), 4.42 (1H, d, H7, $J_{7,7'}$ 14.9), 4.52 (1H, d, H7' $J_{7',7}$ 14.9), 4.62 (1H, dd, H3, $J_{3,2}$ 2.5, $J_{3,4}$ 7.0), 4.69 (1H, dd, H4, $J_{4,5}$ 4.2, $J_{4,3}$ 7.0), 5.19 (1H, d, H2, $J_{2,3}$ 2.5), 5.49 (1H, d, H5, $J_{5,4}$ 4.2); δ_C (100.6 MHz, $CDCl_3$): -5.4, -5.2 ($SiCH_3$); 18.4 ($SiC(CH_3)_3$), 24.9, 25.5 ($C(CH_3)_2$), 25.9 ($SiC(CH_3)_3$), 62.5 (C2), 65.4 (C7), 71.7 (C5), 73.2 (C3), 74.4 (C4), 114.2 ($C(CH_3)_2$), 168.0 (C6), 177.4 (C1); *m/z* (ESI +ve): 705 ([2M+Na]$^+$, 100%).

2,6-((Benzyloxy)carbonyl)amino-7-*O*-*tert*-butyldimethylsilyl-2,6-deoxy-3,4-*O*-isopropylidene-D-*glycero*-D-*talo*-heptono-1,5-lactone S5

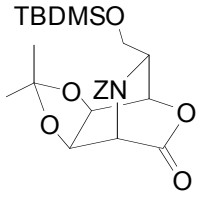

Benzylchloroformate (88 mg, 0.52 mmol, 0.07 mL) in chloroform (1 mL) was added dropwise to a stirred solution of bicyclic imine **S4** (88 mg, 0.26 mmol) and bis(triphenylphosphine) copper(I) tetrahydroborate (187 mg, 0.31 mmol) in chloroform (2 mL) and left to react at rt for 5 h. The reaction was followed by t.l.c. (3:1, cyclohexane/ethyl acetate, starting material R_f 0.36, product, R_f 0.56) and on completion diethyl ether (30 mL) was added. Scratching of the reaction vessel walls lead to formation of a white precipitate on standing. The precipitate was filtered off and washed with diethyl ether (2 x 25 mL) and the combined organic fractions were evaporated to dryness to yield the crude reaction mixture (405 mg). The crude reaction product **S5** was purified *via* flash column chromatography (6:1 → 5:1, cyclohexane/ethyl acetate) and was isolated as a clear oil (111 mg, 0.232 mmol, 90%); HRMS (ESI +ve): found 500.2073 ([M+Na]$^+$); $C_{24}H_{35}NNaO_7Si$ requires: 500.2075;

$[\alpha]_D^{25}$ -14.1 (*c* 1.25 in $CHCl_3$); ν_{max} (thin film): 1787 (s, OC=O), 1715 (s, NC=O); δ_H (400 MHz, $CDCl_3$): 0.04 (6H, 2 x s, $Si(CH_3)_2$), 0.89 (9H, s, $SiC(CH_3)_3$), 1.38, 1.57 (2 x 3H, 2 x s, $C(CH_3)_2$), 3.97 (1H, a-s, H6), 4.18 (1H, a-t, H7, $J_{7,6} = J_{7,7'}$ 9.6), 4.39 (1H, a-s, H7'), 4.50 (1H, dd, H3, $J_{3,2}$ 2.5, $J_{3,4}$ 7.8), 4.59-4.53 (1H, m, H4), 5.06 (1H, a-s, H2), 5.11 (1H, a-s, H5), 5.14 (1H, d, H8, $J_{8,8'}$ 12.4), 5.22 (1H, d, H8', $J_{8',8}$ 12.3), 7.19-7.49 (5H, m, ArH); δ_C (100.6 MHz, $CDCl_3$): -5.4, -5.2 ($Si(CH_3)_2$), 18.3 ($SiC(CH_3)_3$), 23.9, 24.9 ($C(CH_3)_2$), 25.9 ($SiC(CH_3)_3$), 54.4 (C2), 58.5 (C6), 60.5 (C7), 68.1 (C8), 71.7 (C4), 72.1 (C3), 73.8 (C5), 113.9 ($C(CH_3)_2$), 128.4, 128.7, 130.0 (ArCH), 134.0, 134.1 (ArCC), 156.0 (NC=O), 167.5 (C1); *m/z* (ESI +ve): 977 ($[2M+Na]^+$, 100%).

2,6-((Benzyloxy)carbonyl)amino-7-*O*-*tert*-butyldimethylsilyl-2,6-deoxy-3,4-*O*-isopropylidene-D-*glycero*-D-*talo*-heptono-methylamide S6

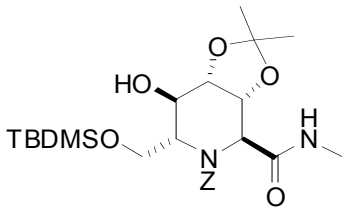

To a solution of bicycle **S5** (40 mg, 0.084 mmol) in dry tetrahydrofuran (1 mL) was added methylamine (33% w/w solution in industrial methylated spirit, 0.25 mmol, 0.03 mL). The reaction was followed by t.l.c. analysis (1:1, cyclohexane/ethyl acetate, starting material R_f 0.82, product R_f 0.33) and on completion of the reaction after 18 h, the solution was concentrated to dryness and purified *via* column chromatography (1:1, cyclohexane/ethyl acetate). The product **S6** was obtained as a white crystalline solid (25 mg, 0.050 mmol, 59%); HRMS (ESI +ve): found 531.2495 ($[M+Na]^+$); $C_{25}H_{40}N_2NaO_7Si$ requires: 531.2497; m.p. 148-152 °C; $[\alpha]_D^{25}$ +10.3 (*c* 0.99, $CHCl_3$); ν_{max} (thin film): 3312 (br, OH), 1702 (s, NC=OO), 1663 (s, amide I), 1570 (w, amide II); δ_H (400 MHz, $CDCl_3$): -0.08 (6H, s, $Si(CH_3)_2$), 0.83 (9H, s, $SiC(CH_3)_3$), 1.31, 1.47 (2 x 3H, s, $C(CH_3)_2$), 2.81 (3H, s, NHMe), 3.67 (1H, a-s, H7),

3.80 (1H, t, H7', $J_{7',6} = J_{7',7}$ 9.7), 4.21 (2H, a-d, H5, H6, J 10.5), 4.39 (1 H, d, H4, $J_{4,3}$ 7.5), 4.54 (1H, d, H3, $J_{3,4}$ 7.5), 4.60 (1H, a-s, H2), 5.06 (1H, d, H8, $J_{8,8'}$ 12.5), 5.22 (1H, d, H8', $J_{8',8}$ 12.5), 6.06 (1H, d, OH, $J_{OH,5}$ 11.5), 6.75 (1H, s, NH), 7.34 (5H, a-s, ArH); δ_C (126 MHz, $CDCl_3$): -5.3, -5.2 ($Si(CH_3)_2$), 18.3 ($SiC(CH_3)_3$), 22.8 (NHMe), 25.0 ($C(CH_3)_2$), 25.9 ($SiC(CH_3)_3$), 26.8 ($C(CH_3)_2$), 57.7 (C2), 59.7 (C6), 62.0 (C7), 65.2 (C5), 68.1 (C8), 72.1 (C3), 73.5 (C4), 107.7 ($C(CH_3)_2$), 128.1, 128.4, 128.5, 128.6, 128.7 (ArCH), 135.8 (ArCC), 157.3 (NC=OO), 173.1 (C1); *m/z* (ESI +ve): 531 ($[M+Na]^+$, 100%).

2,6-Dideoxy-2,6-imino-D-*glycero*-D-*talo*-heptono-methylamide 10

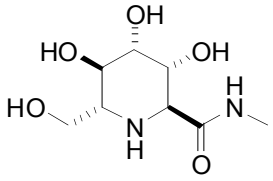

Carbamate **S6** (17 mg, 0.03 mmol) was put in 3% methanolic hydrochloric acid and the disappearance of the starting material was monitored by t.l.c. (1:1, cyclohexane/ethyl acetate, starting material R_f 0.26, product baseline). The starting material had been completely converted after 4 h and 10% palladium on charcoal (10% by weight, 2 mg) was added and the reaction was followed by mass spectrometry. After 18 h the reaction mixture was filtered (glass microfiber) and subjected to ion exchange chromatography (Amberlite IR120, H^+ form, eluting with 1.0 M aq. ammonium hydroxide), to give the product **10** as a clear oil (7 mg, 95%); HRMS (ESI +ve): found 221.1131 ($[M+H]^+$); $C_8H_{17}N_2O_5$ requires: 221.1132; $[\alpha]_D^{25}$ -7.1 (*c* 0.59, H_2O); [Lit.[5] $[\alpha]_D^{22}$ -10.0 (*c* 0.66, H_2O)]; ν_{max} (thin film): 3383 (br, NH, OH), 1651 (s, amide I), 1539 (m, amide II); δ_H (400 MHz, D_2O): 2.65 (1H, ddd, H6, $J_{6,7'}$ 3.1, $J_{6,7}$ 5.4, $J_{6,5}$ 9.3), 2.77 (3H, s, Me), 3.47 (1H, dd, H4, $J_{4,3}$ 2.9, $J_{4,5}$ 9.5), 3.59 (1H, a-t, H5, $J_{5,4} = J_{5,6}$ 9.4), 3.77-3.67 (2H, m, H7, H2), 3.81 (1H, dd, H7', $J_{7',6}$ 3.1, $J_{7',7}$ 11.6), 4.43 (1 H, a-t, H3, $J_{3,2} = J_{3,4}$ 2.9); δ_C (100.6 MHz, D_2O): 26.3 (Me), 58.1 (C6), 60.9 (C2), 61.7 (C7), 68.4 (C5), 70.3 (C3), 72.9 (C4), 173.4 (C1); *m/z* (ESI +ve): 243 ($[M+Na]^+$, 100%).

Experimental for pyrrolidine amides

2-Azido-2-deoxy-D-lyxono-1,4-lactone 22

Benzylidene lactone **24** (1.71 g, 7.2 mmol) was dissolved in a mixture of trifluoroacetic acid (50 mL), 1,4-dioxane (50 mL) and water (50 mL) and stirred at rt for 4 h. After this time t.l.c. analysis (ethyl acetate) showed complete conversion of the starting material (R_f 0.60), to one major product (R_f 0.30). The reaction mixture was diluted with water (50 mL) and the solvent removed under reduced pressure, co-evaporating with water (5 x 25 mL) Purification by flash column chromatography (1:1, cyclohexane/ethyl acetate) yielded the unprotected lactone **22** (1.0 g, 88%) as a colourless oil; $[\alpha]_D^{25}$ +41.3 (*c* 0.60, H_2O) [Lit.[7] $[\alpha]_D^{20}$ +38.0 (*c* 0.25, H_2O)]; ν_{max} (thin film): 3385 (br. s, OH), 2120 (s, N_3), 1778 (s, C=O); δ_H (400 MHz, $(CD_3)_2CO$): 3.92 (2H, a-t, H5, H5', *J* 5.6), 4.23 (1H, t, OH5, $J_{OH,5}$ 5.8), 4.39 (1H, d, H2, $J_{2,3}$ 4.6), 4.56 (1H, dt, H4, $J_{4,3}$ 2.8, $J_{4,5} = J_{4,5'}$ 5.8), 4.75 (1H, dt, H3, $J_{3,4}$ 2.8, $J_{3,2} = J_{3,OH}$ 4.6), 5.36 (1H, d, OH3, $J_{OH,3}$ 4.6); δ_C (100.6 MHz, $(CD_3)_2CO$): 59.7 (C5), 62.0 (C2), 70.9 (C3), 81.9 (C4), 171.5 (C1); *m/z* (ESI +ve): 174 ($[M+H]^+$, 100%)

[Enantiomer: **2-Azido-2-deoxy-L-lyxono-1,4-lactone** $[\alpha]_D^{25}$ -21.9 (*c* 1.20, H_2O)].

1,4-Dideoxy-1,4-imino-D-arabinitol, DAB 27

Sodium borohydride (36 mg, 0.95 mmol) was added to a solution of the crude bicyclic salt (50 mg, 0.18 mmol) in ethanol (2 mL). The reaction was stirred for 12 h at rt after which mass spectrometry indicated the presence of the product (*m/z* 134 ($M+H^+$)). The solvent was removed under reduced pressure and the residue loaded onto a short column of Dowex® (50W X8, H^+). The column was washed with water and the product liberated with 2 M aqueous ammonia. The ammoniacal fractions were concentrated under reduced pressure to give pyrrolidine **27** (15 mg, 63%) as a brown oil; HRMS (ESI +ve): found 134.0812 ($[M+H]^+$); $C_5H_{12}NO_3$ requires 134.0812; $[\alpha]_D^{25}$ +8.5 (*c* 0.30, H_2O) [Lit.[8] $[\alpha]_D^{25}$ +8.2 (*c* 0.25,

H_2O)]; ν_{max} (thin film): 3276 (br. s, OH/NH); δ_H (400 MHz, D_2O, HCl Salt): 3.30 (1H, br. a-d, H1, J_{gem} 12.1), 3.49-3.58 (2H, m, H1', H4), 3.82 (1H, ddd, H5, *J* 1.5, *J* 8.1, J_{gem} 12.1), 3.94 (1H, ddd, H5', *J* 1.8, *J* 4.7, J_{gem} 12.0), 4.05-4.09 (1H, br. m, H3), 4.32 (1H, ddd, H2, *J* 1.8, *J* 3.0, *J* 4.8); δ_C (100.6 MHz, D_2O, HCl Salt): 50.7 (C1), 60.0 (C5), 67.0 (C4), 75.3 (C3), 76.7 (C2); *m/z* (ESI +ve): 134 ($[M+H]^+$, 100%).

[Enantiomer: **1,4-Dideoxy-1,4-imino-L-arabinitol, LAB** $[\alpha]_D^{25}$ -8.5 (*c* 0.30, H_2O)]

2,5-Dideoxy-2,5-imino-D-lyxonoic acid 28

Azido triflate (0.21 g, 0.69 mmol) and palladium black (20 mg) were stirred at rt in ethyl acetate (5 mL). The reaction vessel was purged under vacuum and charged with an atmosphere of hydrogen and stirred for 2 h. 2 M Hydrochloric acid (2.1 mL) was added and the reaction was stirred for a further 14 h after which mass spectrometry indicated the presence of the product (*m/z* 170 $[M+Na]^+$). The catalyst was removed by filtration (glass microfibre). The solvent was removed under reduced pressure and the residue loaded onto a short column of Dowex® (50W-X8, H^+). The column was washed with water and the product liberated with 2 M aqueous ammonia. The ammoniacal fractions were concentrated under reduced pressure to give the amino acid **28** (92 mg, 90%) as a yellow solid; HRMS (ESI +ve): found 170.0429 ($[M+Na]^+$); $C_5H_9NNaO_4$ requires 170.0424; $[\alpha]_D^{25}$ -11.8 (*c* 0.25, H_2O) [Lit.[9] $[\alpha]_D^{25}$ -12.2 (*c* 0.83, H_2O)]; ν_{max} (thin film): 3465 (br. m, OH), 3254 (br. m, OH), 3110 (br. m, OH), 2970 (br. s, NH), 1738 (C=O); δ_H (400 MHz, D_2O, HCl Salt): 3.52 (1H, ddd, H5, $J_{5,3}$ 1.0, $J_{5,4}$ 1.8, $J_{5,5'}$ 12.9), 3.60 (1H, dd, H5', $J_{5',4}$ 3.8, $J_{5',5}$ 12.6), 4.06-4.07 (1H, m, H2), 4.31 (1H, dt, H4, $J_{4,3} = J_{4,5}$ 1.5, $J_{4,5'}$ 3.6), 4.52 (1H, a-q, H3, $J_{3,2} = J_{3,4} = J_{3,5}$ 1.3); δ_C (100.6 MHz, D_2O, HCl Salt): 51.6 (C5), 68.2 (C2), 74.6 (C4), 79.0 (C3), 171.8 (C1); *m/z* (ESI +ve): 170 ($[M+Na]^+$, 100%).

[Enantiomer: **2,5-Dideoxy-2,5-imino-L-lyxonoic acid** $[\alpha]_D^{25}$ +5.9 (*c* 0.27, H_2O)].

8. NMR Spectra

2-Azido-7-*O*-*tert*-butyldimethylsilyl-2-deoxy-3,4-*O*-isopropylidene-D-*talo*-6-heptulosono-1,5-lactone S3

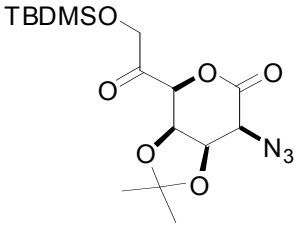

^{1}H (400 MHz, $CDCl_3$)

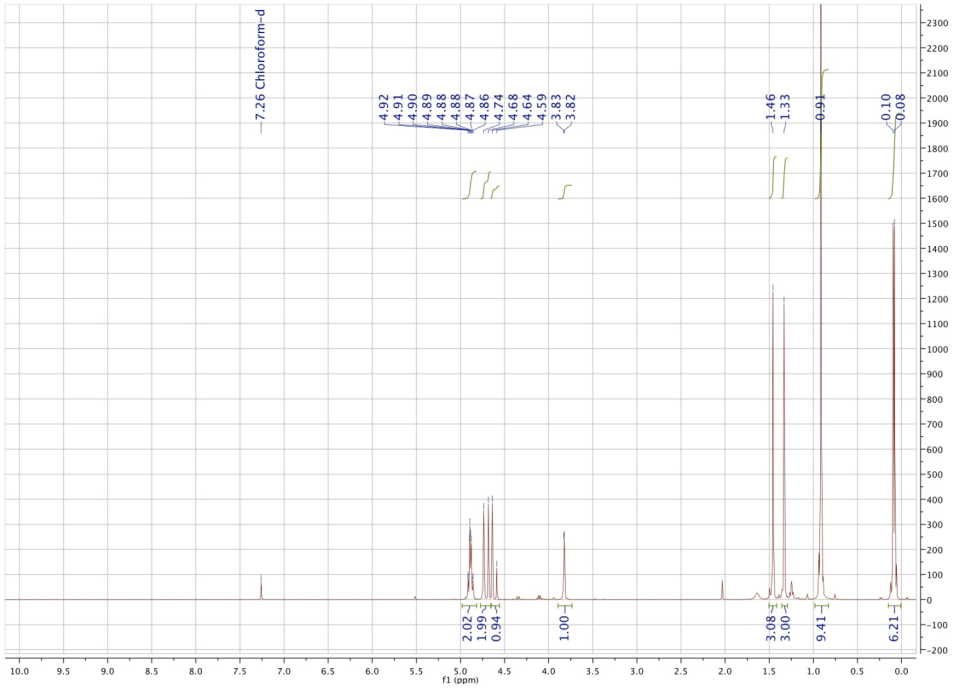

^{13}C (100.6 MHz, $CDCl_3$)

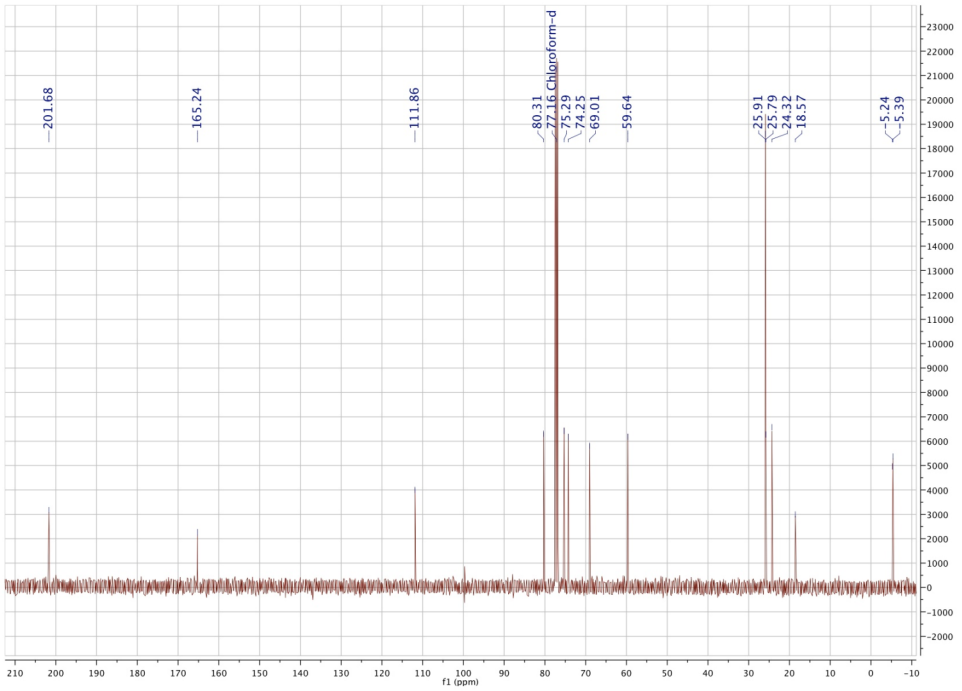

7-*O*-*tert*-Butyldimethylsilyl-2,6-deoxy-2,6-imino-3,4-*O*-isopropylidene-D-*talo*-6-heptulosono-1,5-lactone S4

TBDMSO

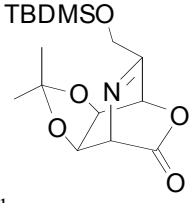

^{1}H (400 MHz, $CDCl_3$)

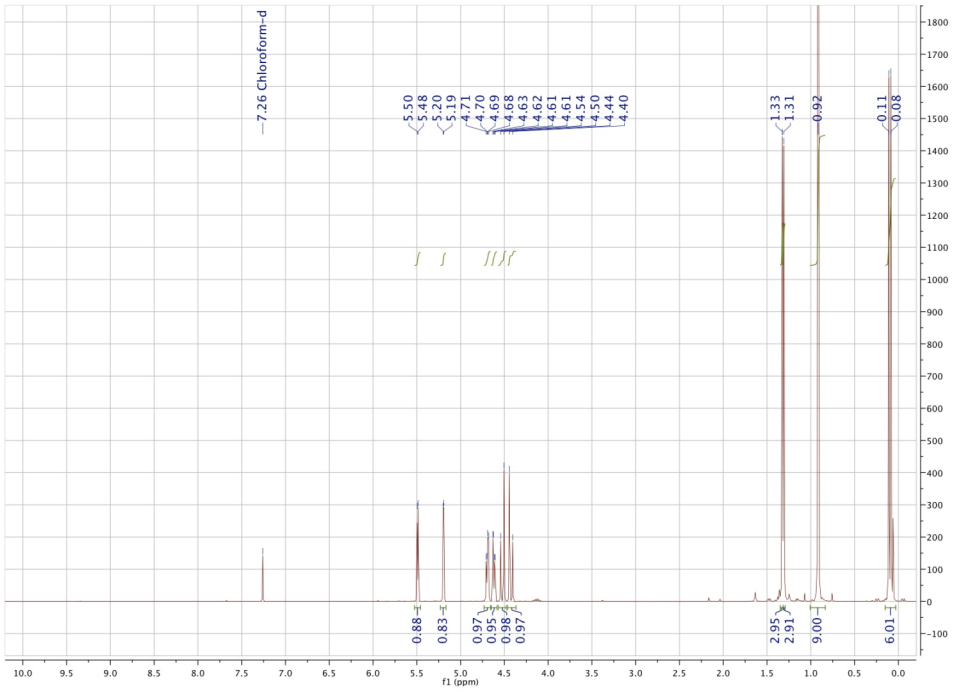

^{13}C (100.6 MHz, $CDCl_3$)

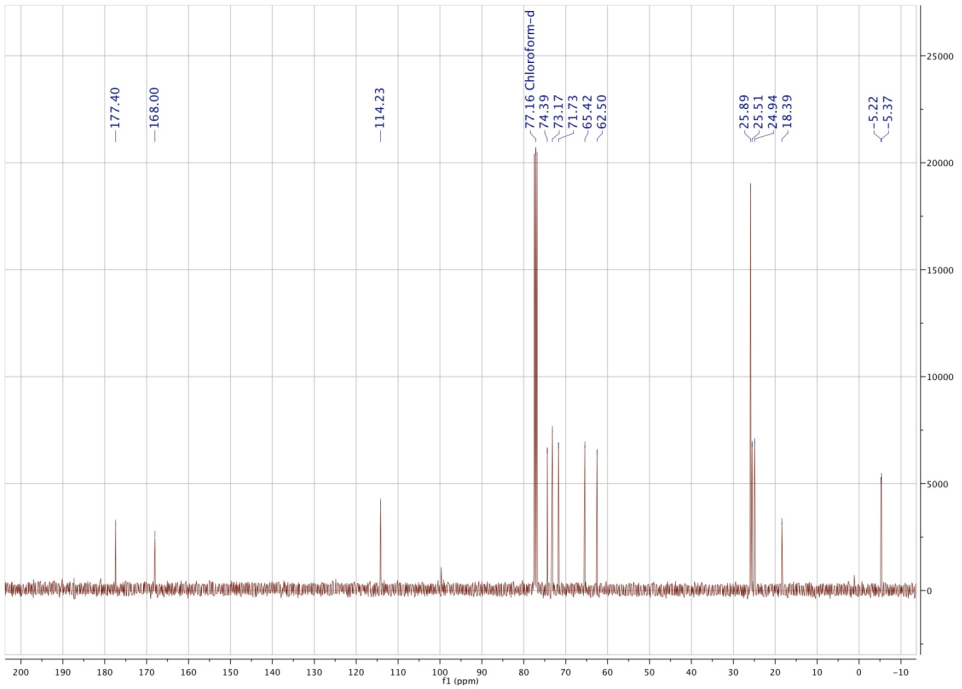

2,6-((Benzyloxy)carbonyl)amino-7-*O-tert*-butyldimethylsilyl-2,6-deoxy-3,4-*O*-isopropylidene-D-*glycero*-D-*talo*-heptono-1,5-lactone S5

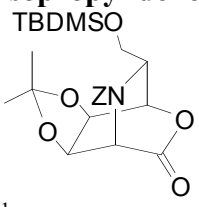

^{1}H (400 MHz, $CDCl_3$)

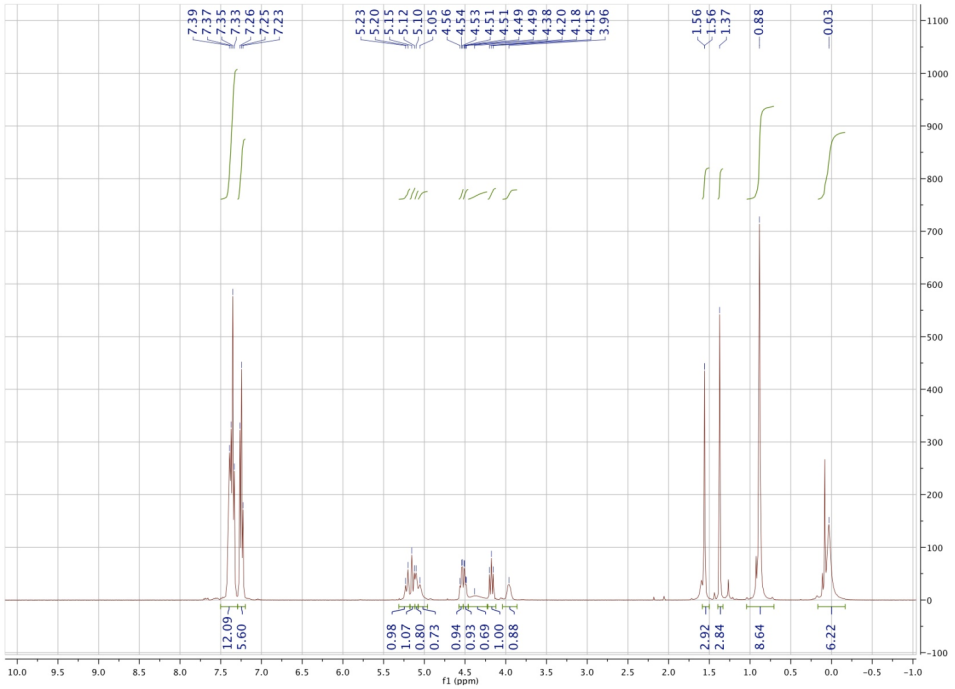

^{13}C (100.6 MHz, $CDCl_3$)

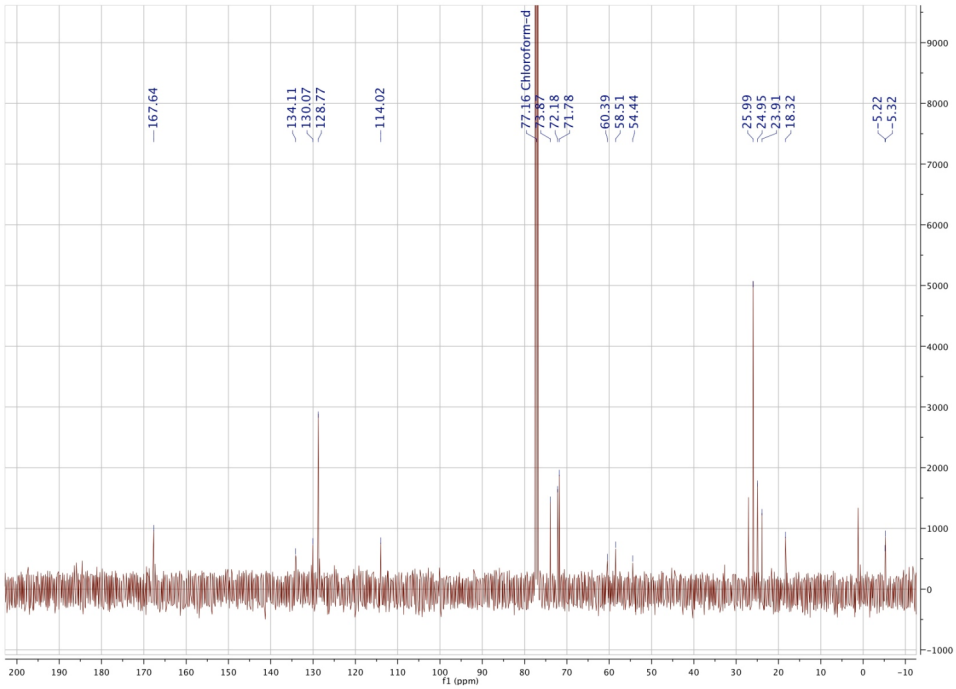

2,6-((Benzyloxy)carbonyl)amino-7-*O*-*tert*-butyldimethylsilyl-2,6-deoxy-3,4-*O*-isopropylidene-D-*glycero*-D-*talo*-heptono-methylamide S6

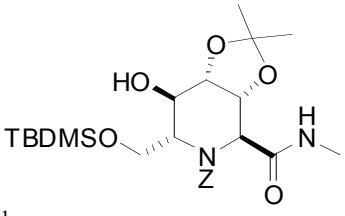

^{1}H (400 MHz, $CDCl_3$)

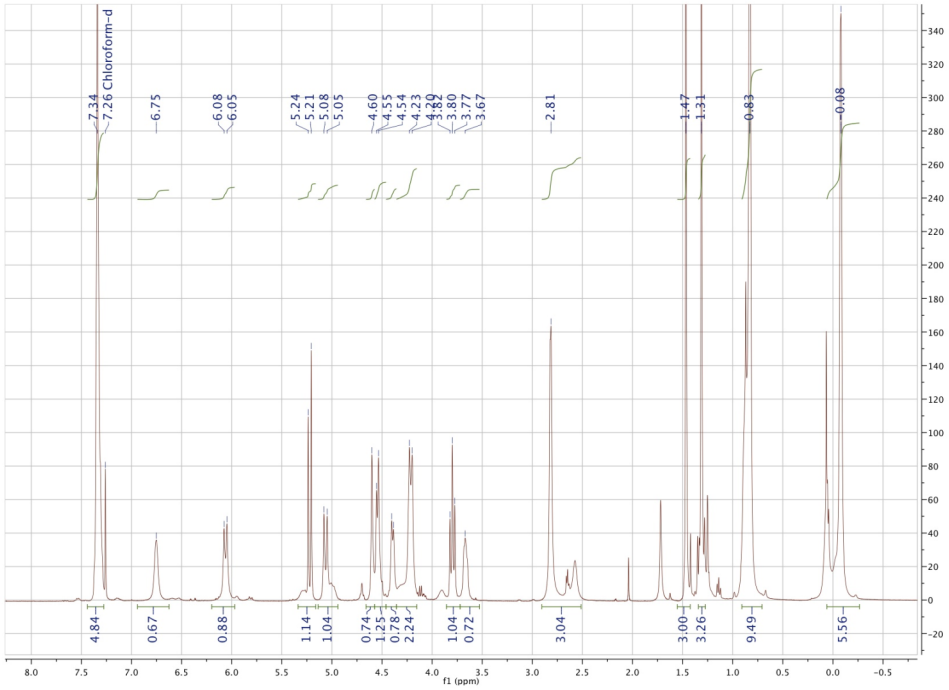

^{13}C (126 MHz, $CDCl_3$)

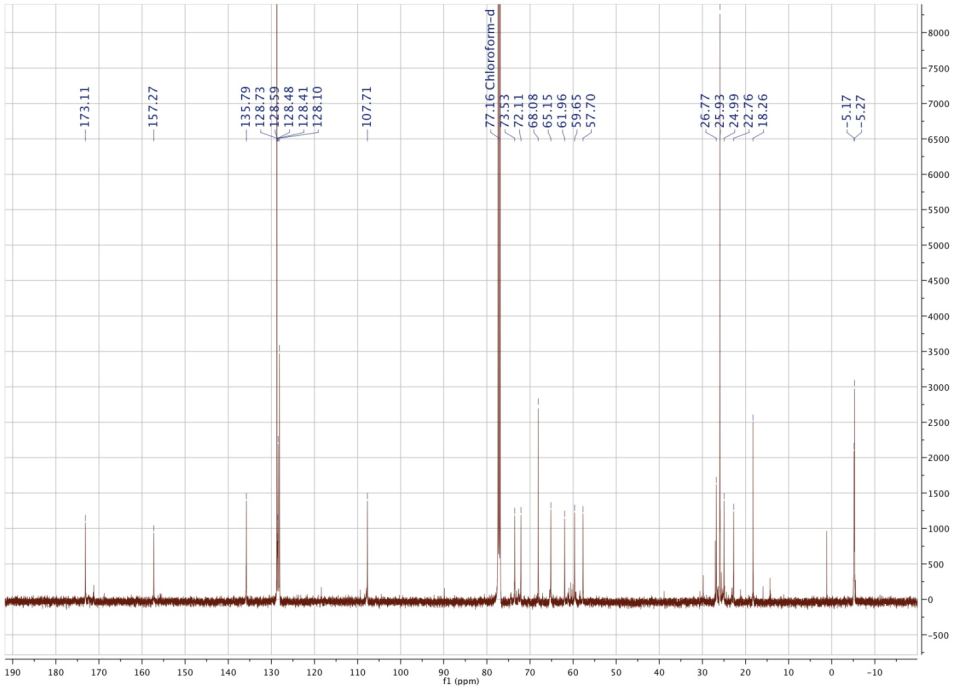

2,6-Dideoxy-2,6-imino-D-*glycero*-D-*talo*-heptono-methylamide 10

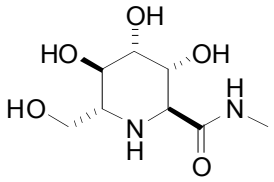

^{1}H (400 MHz, D_2O)

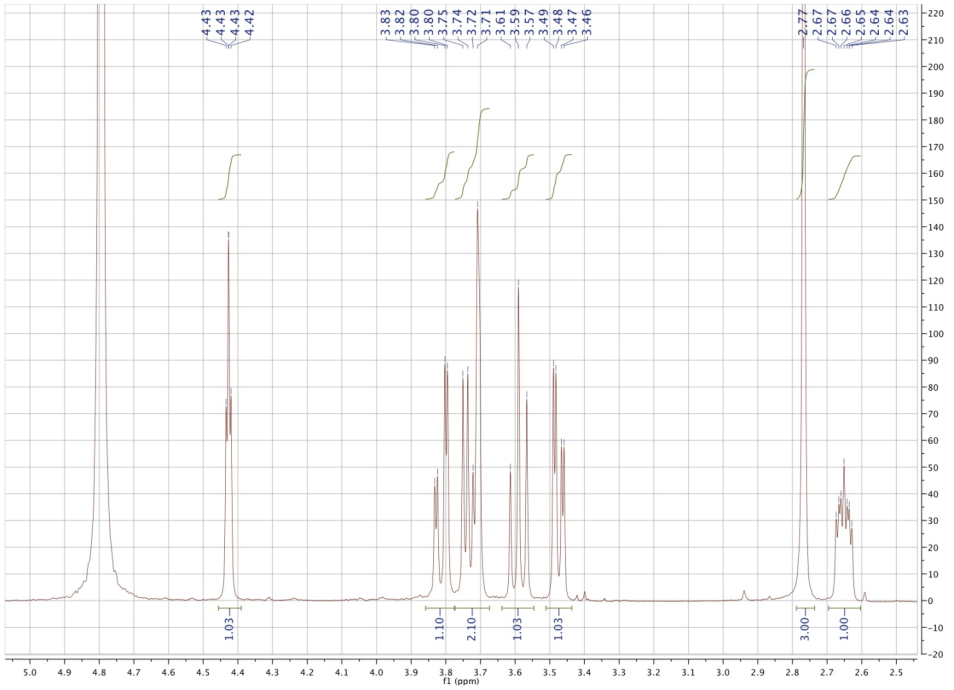

^{13}C (100.6 MHz, D_2O)

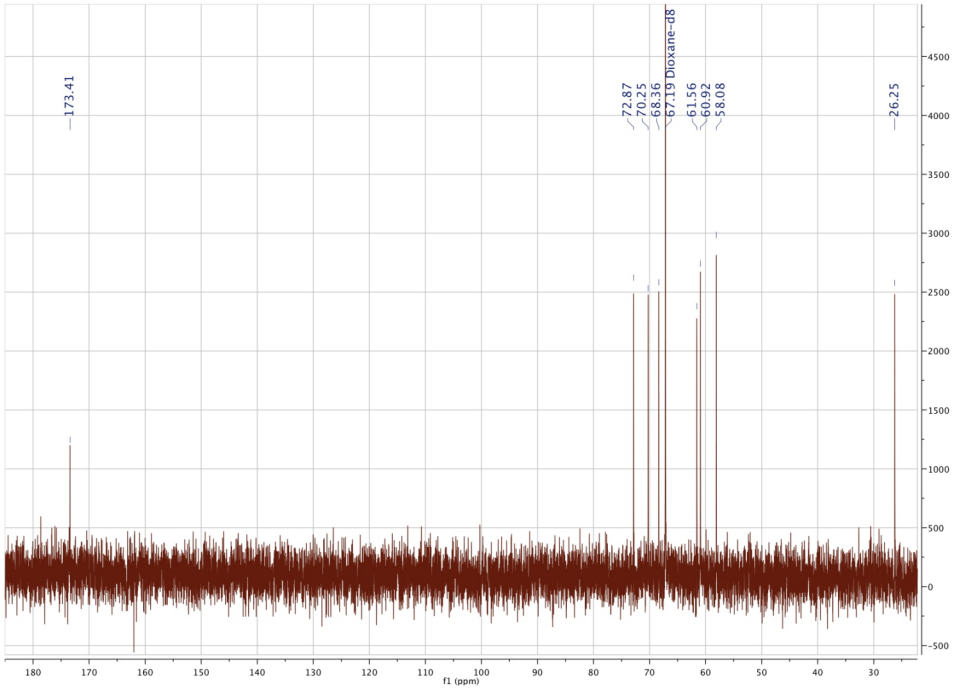

7-*O*-*tert*-Butyldimethylsilyl-2,6-dideoxy-2,6-imino-3,4-*O*-isopropylidene-L-*glycero*-D-*talo*-heptono-1,5-lactone 19

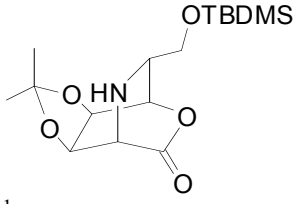

^{1}H (400 MHz, $CDCl_3$)

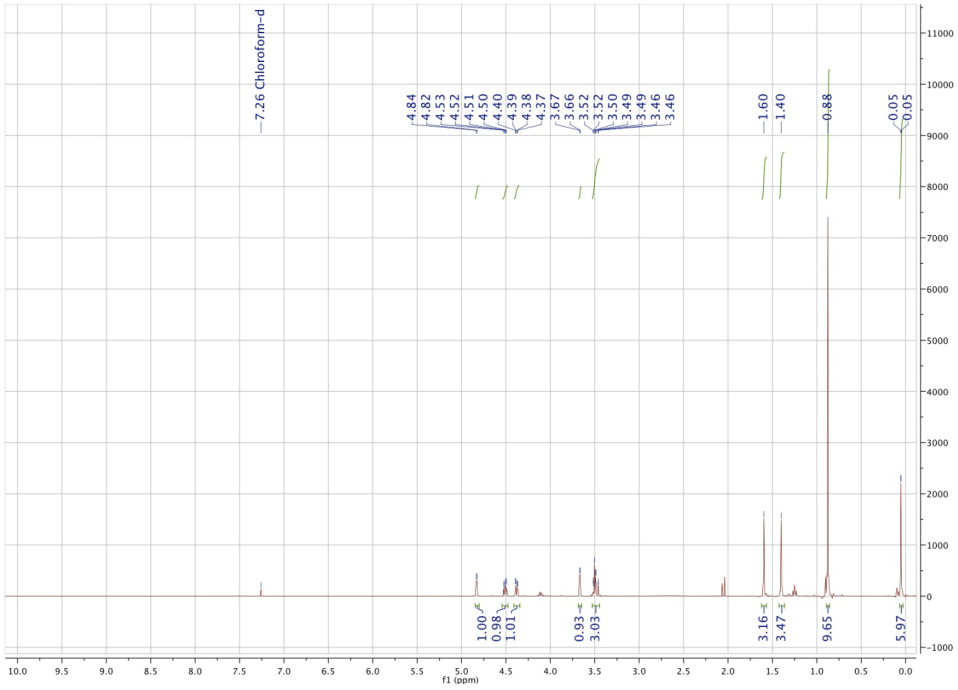

^{13}C (100.6 MHz, $CDCl_3$)

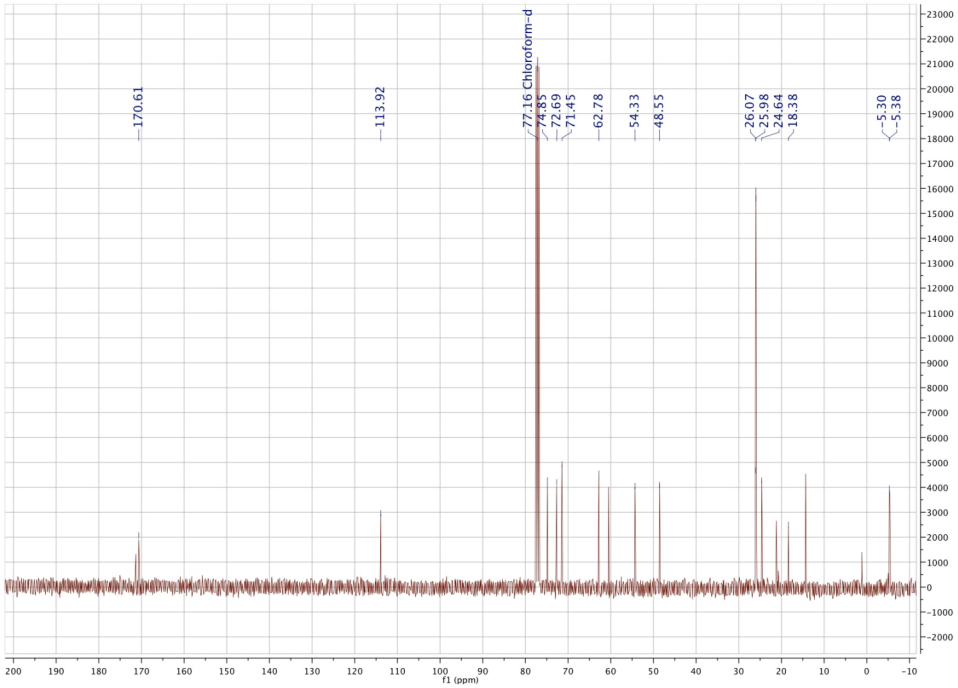

Methyl 7-*O*-*tert*-butyldimethylsilyl-2,6-dideoxy-2,6-imino-3,4-*O*-isopropylidene-L-*glycero*-D-*talo*-heptonamide 20

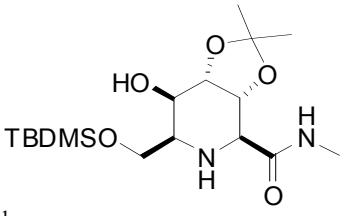

^{1}H (400 MHz, $CDCl_3$)

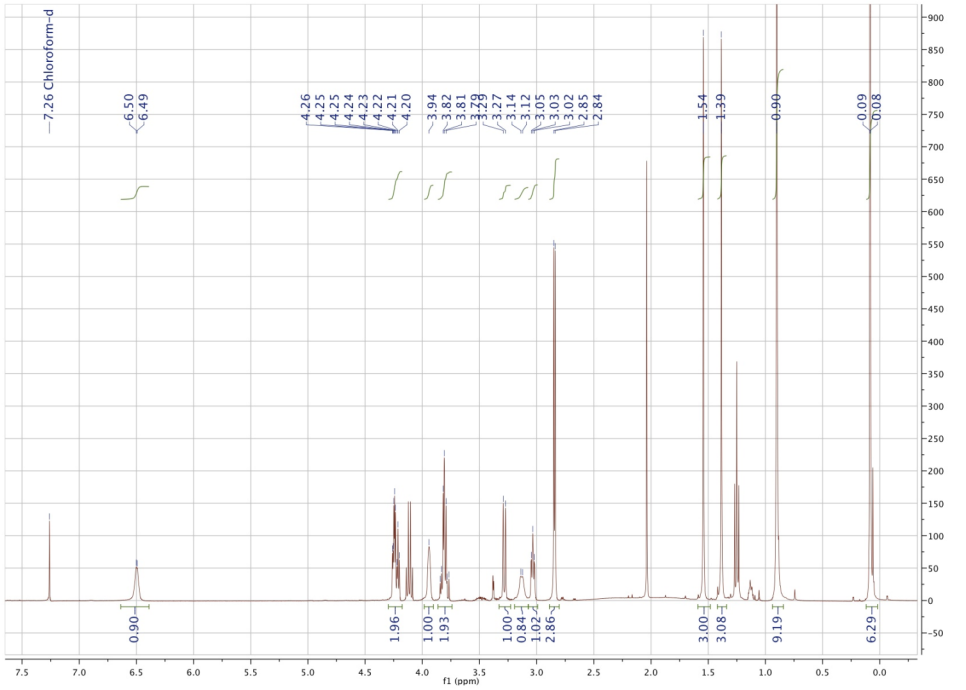

^{13}C (100.6 MHz, $CDCl_3$)

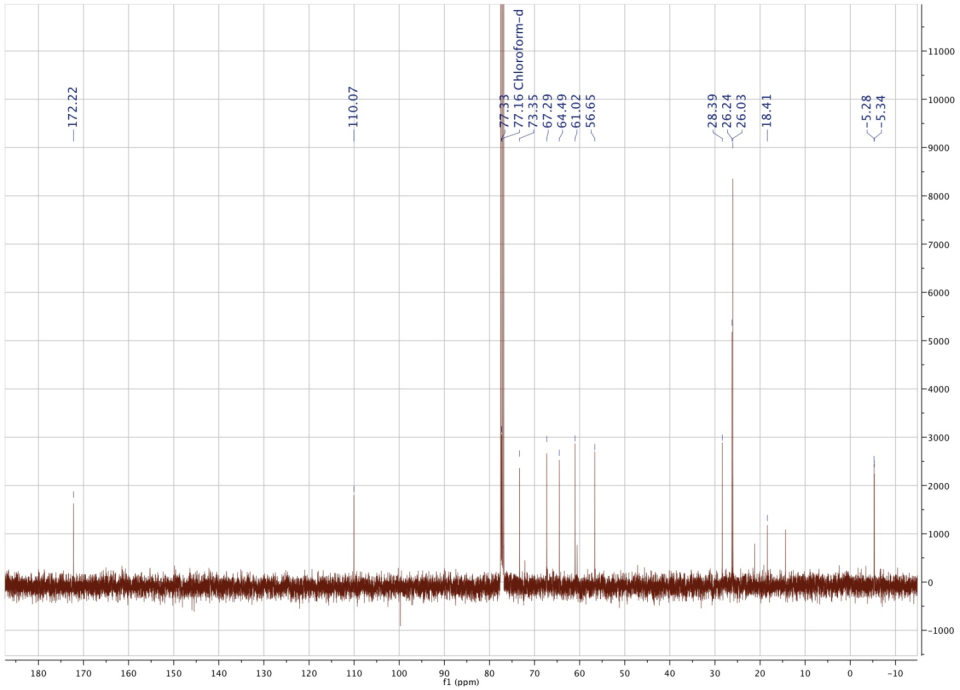

Methyl 2,6-dideoxy-2,6-imino-L-*glycero*-D-*talo*-heptonamide 13

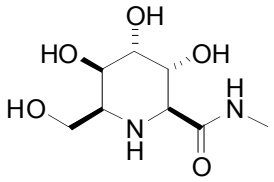

^{1}H (400 MHz, D_2O)

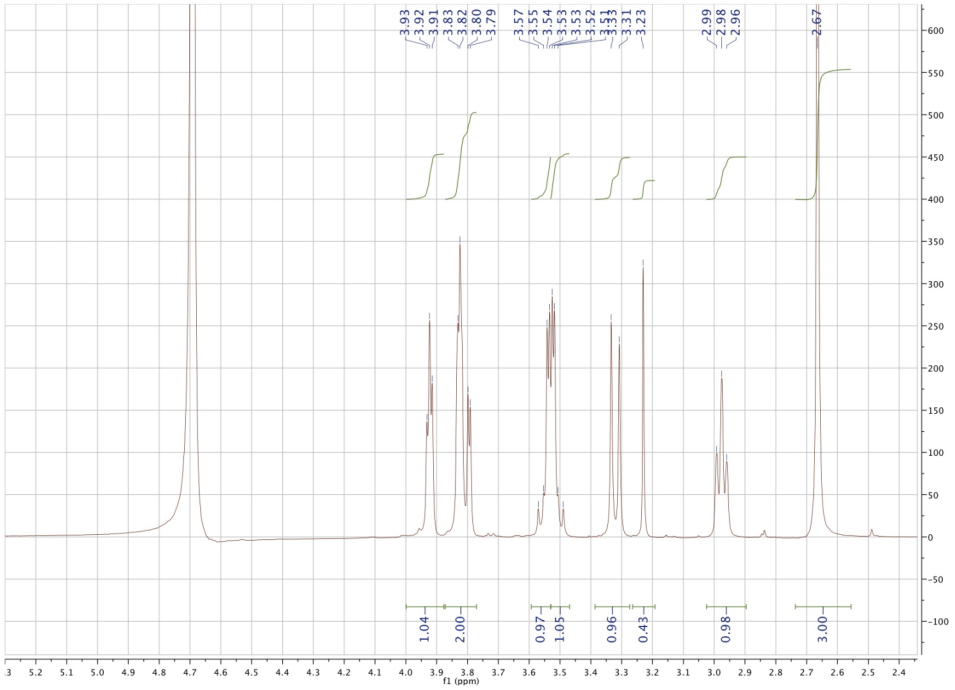

^{13}C (100.6 MHz, D_2O)

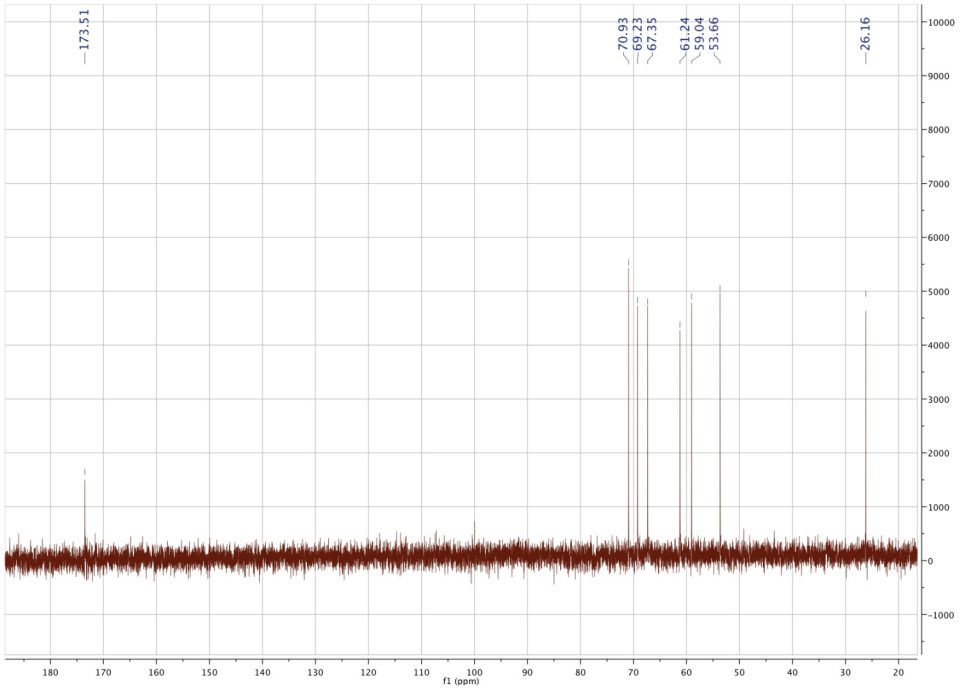

2-Azido-2-deoxy-D-lyxono-1,4-lactone 22

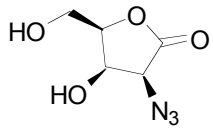

^{1}H (400 MHz, $(CH_3)_2CO$)

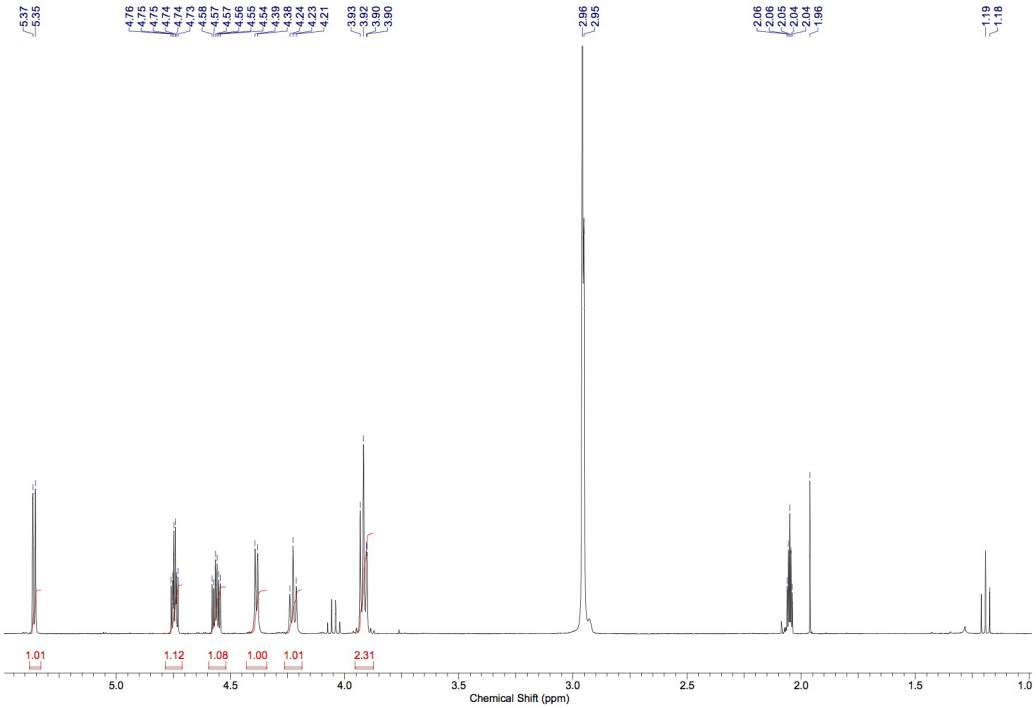

^{13}C (100.6 MHz, $(CH_3)_2CO$)

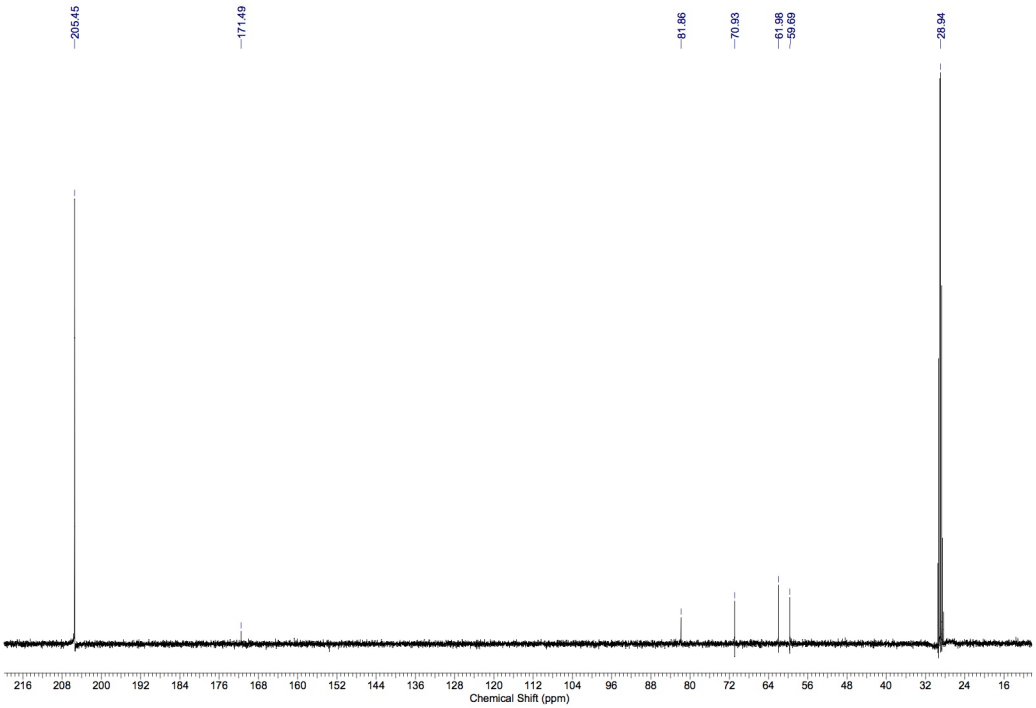

2-Azido-2-deoxy-5-*O*-trifluoromethanesulfonyl-D-lyxono-1,4-lactone 25

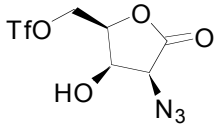

^{1}H (400 MHz, $(CH_3)_2CO$)

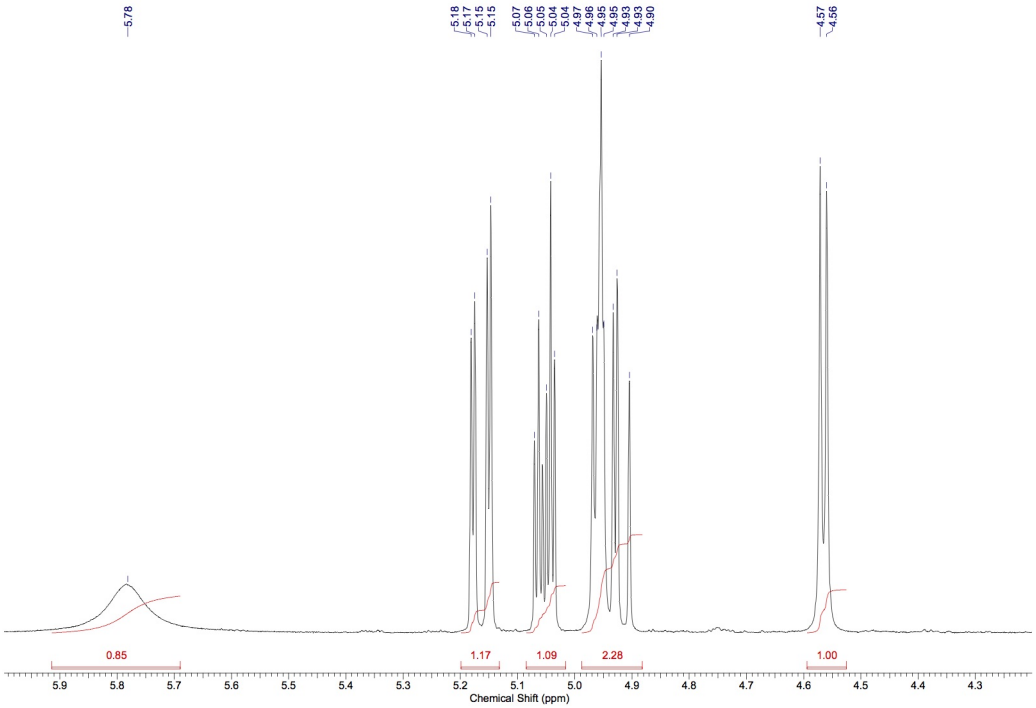

^{13}C (100.6 MHz, $(CH_3)_2CO$)

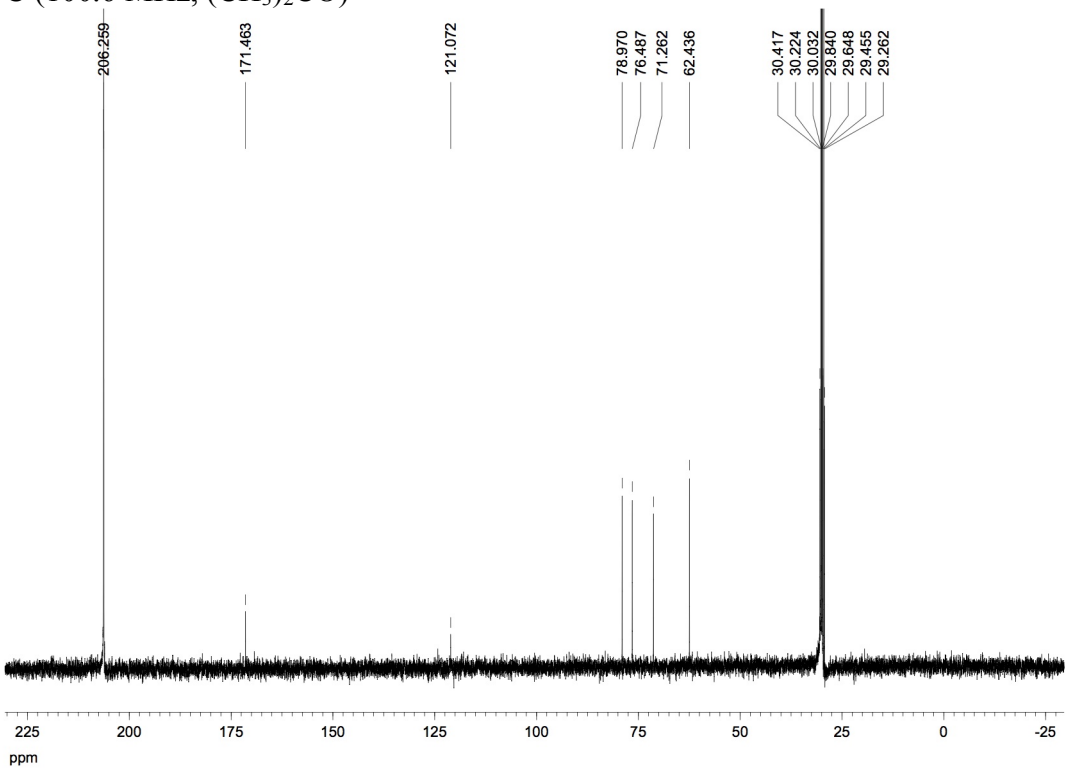

1,4-Dideoxy-1,4-imino-D-arabinitol, DAB [HCl Salt] 27

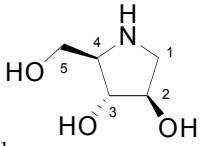

^{1}H (400 MHz, D_2O)

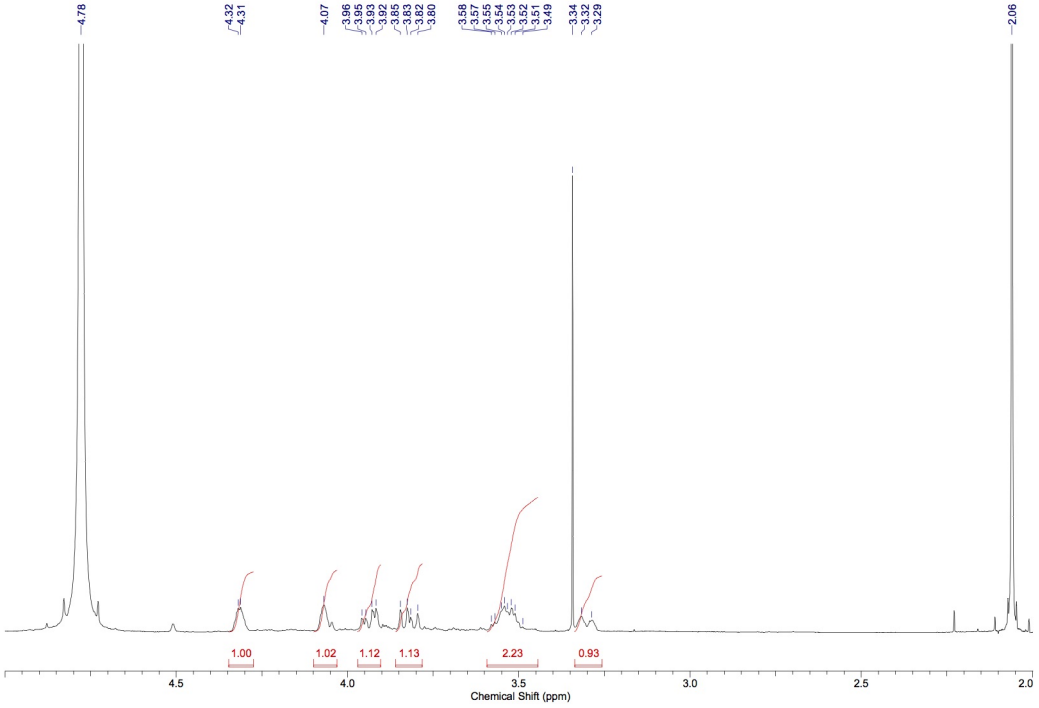

^{13}C (100.6 MHz, D_2O)

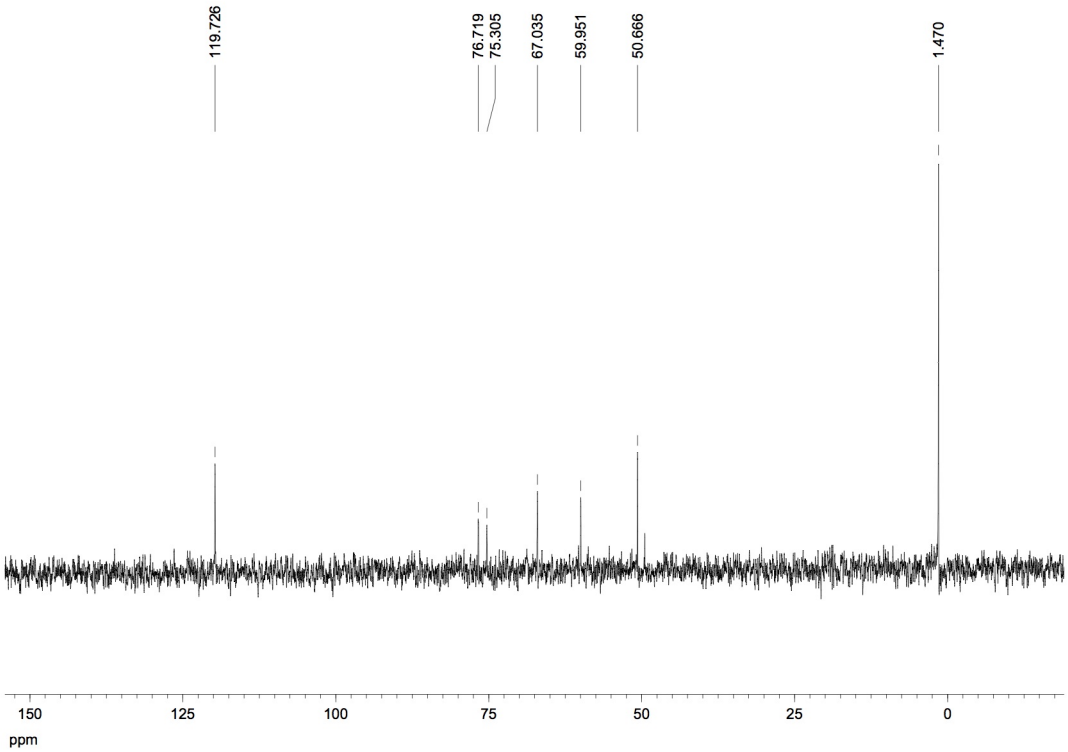

Methyl 2,5-dideoxy-2,5-imino-D-lyxonamide [HCl Salt] 21

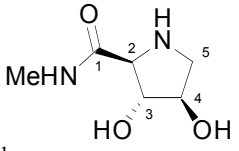

^{1}H (400 MHz, D_2O)

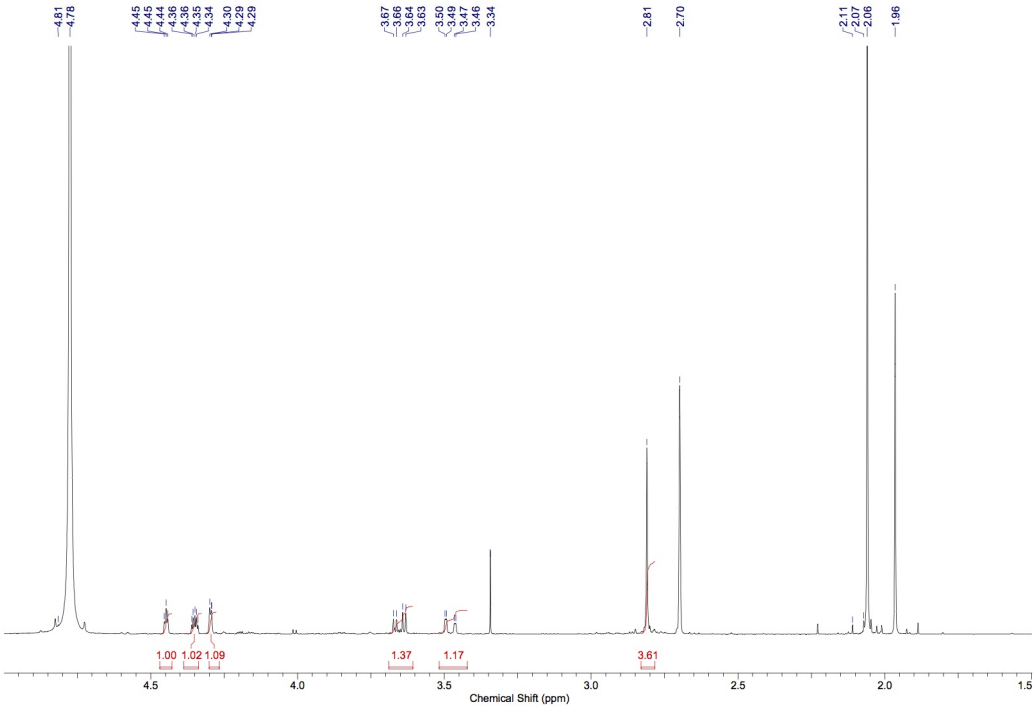

^{13}C (100.6 MHz, D_2O)

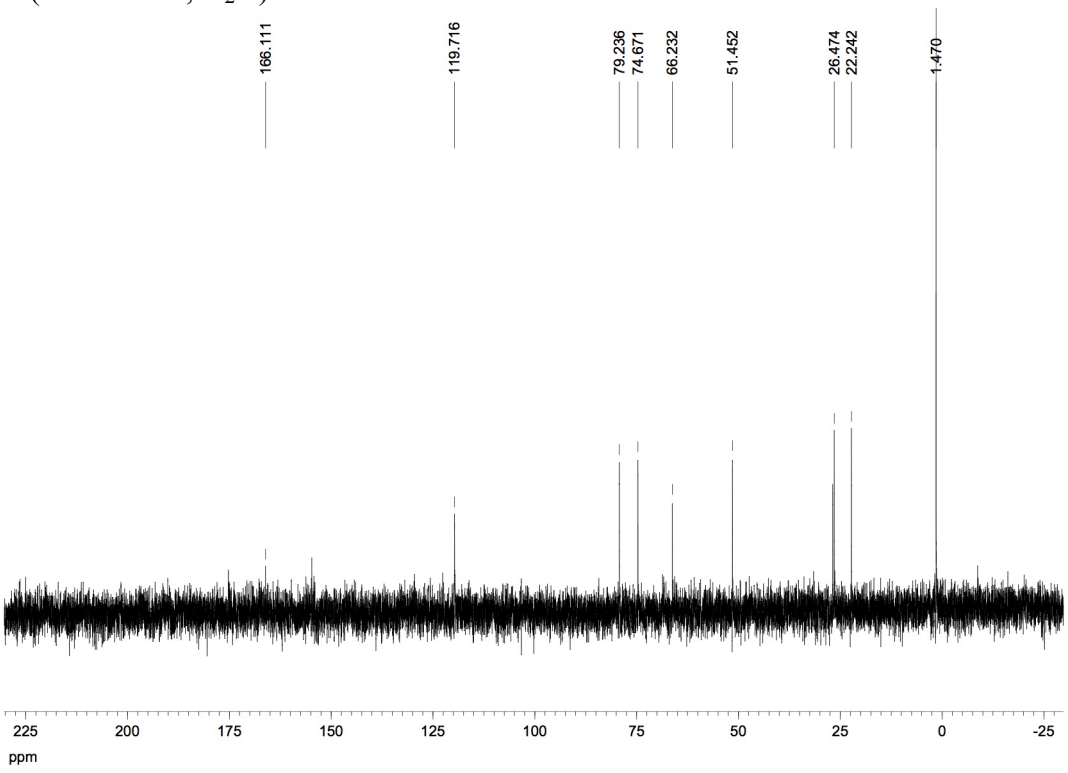

2,5-Dideoxy-2,5-imino-D-lyxonoic acid [HCl Salt] 28

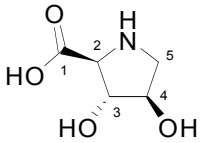

^{1}H (400 MHz, D_2O)

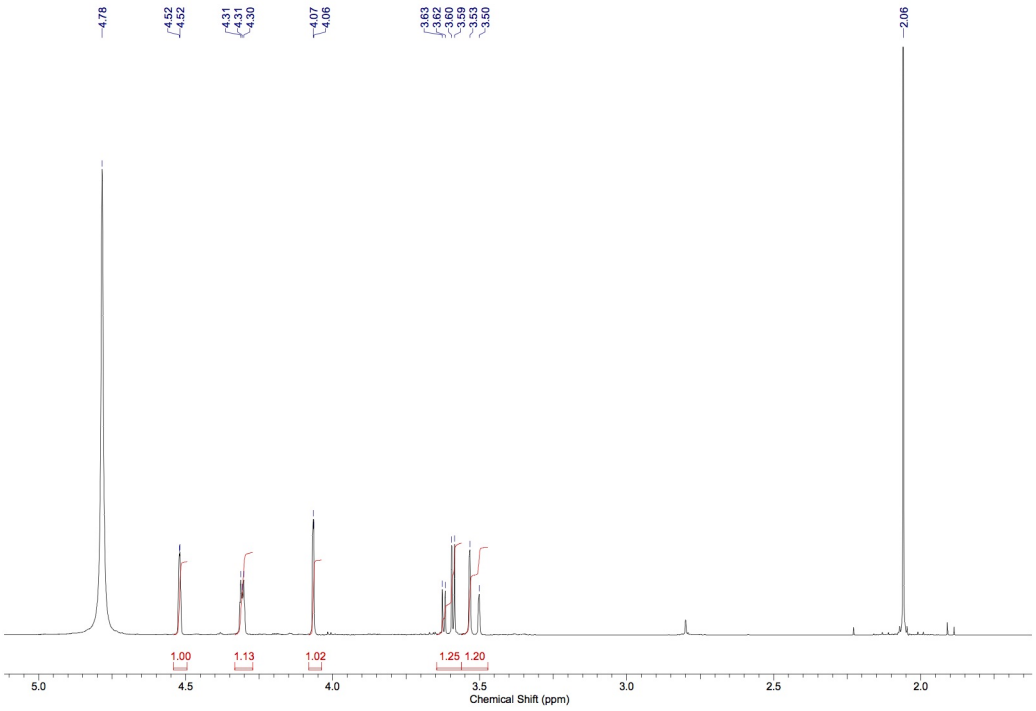

^{13}C (100.6 MHz, D_2O)

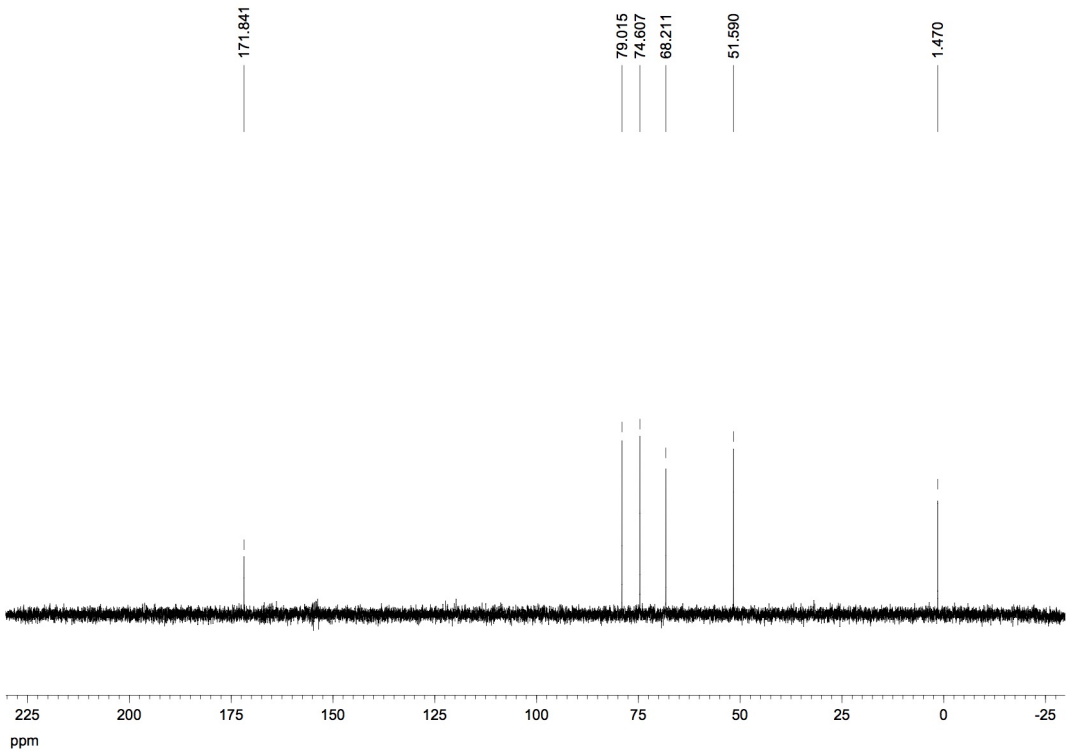

Methyl *N*-butyl-2,5-dideoxy-2,5-imino-D-mannonamide 35

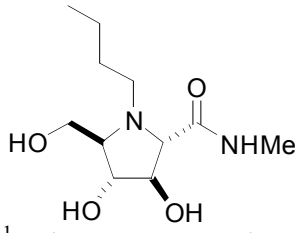

^{1}H (400 MHz, D_2O)

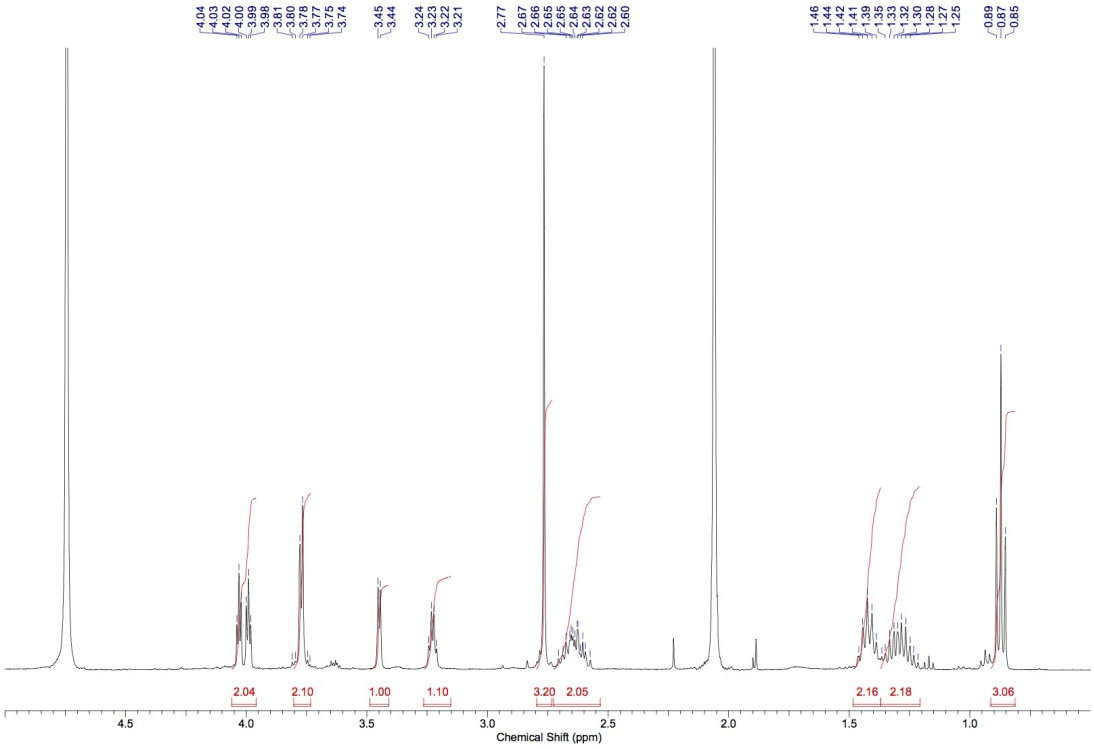

^{13}C (100.6 MHz, D_2O)

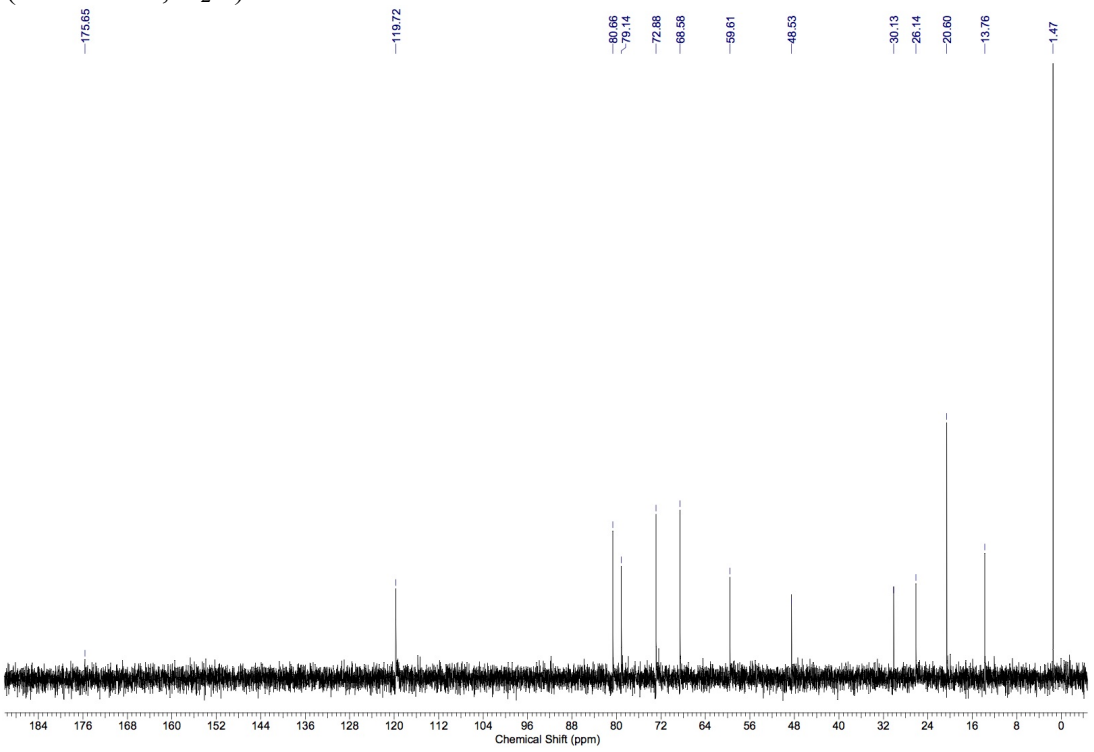

Methyl *N*-hydroxyethyl-2,5-dideoxy-2,5-imino-D-mannonamide 36

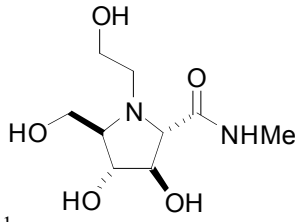

^{1}H (400 MHz, D_2O)

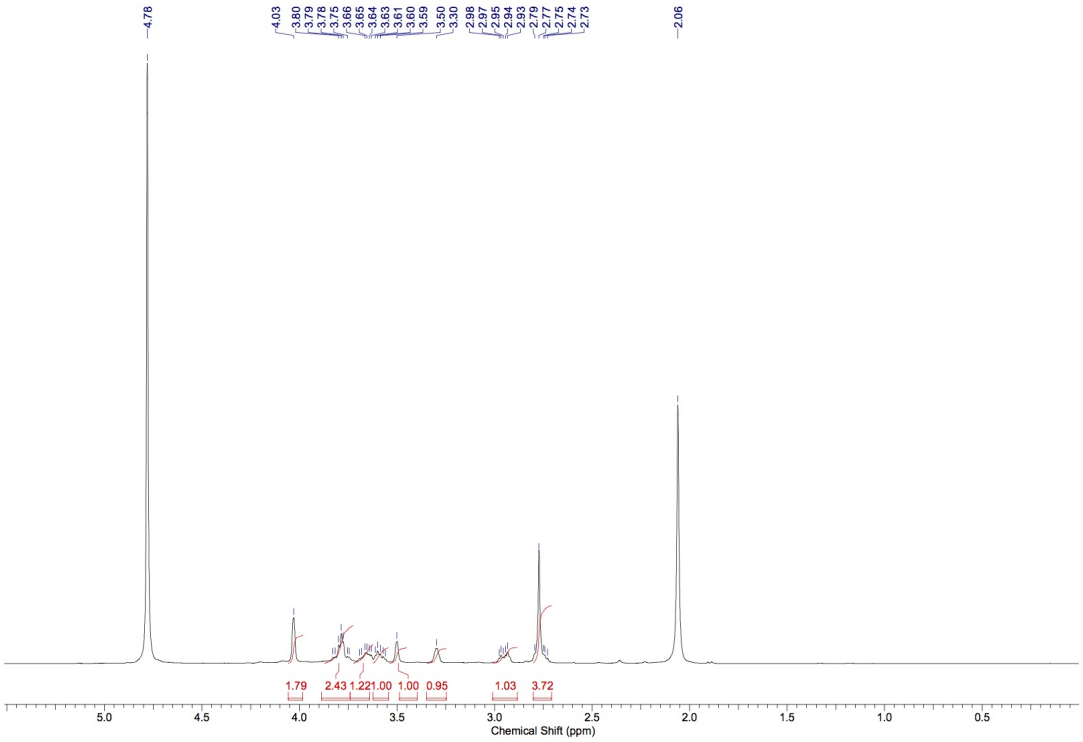

^{13}C (125.6 MHz, D_2O)

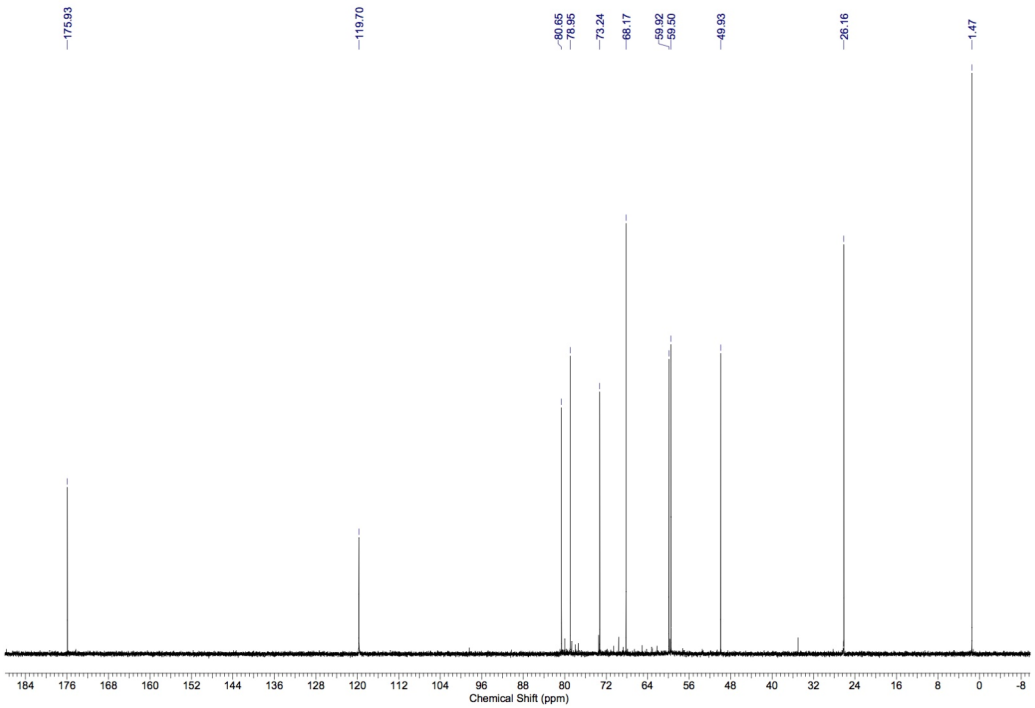

Methyl *N′*-[2-Carboxyethyl]-2,5-dideoxy-2,5-imino-D-mannonamide 37

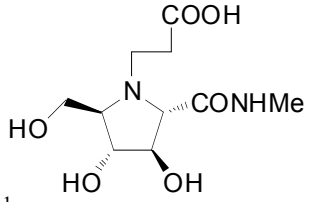

^{1}H (400 MHz, D_2O)

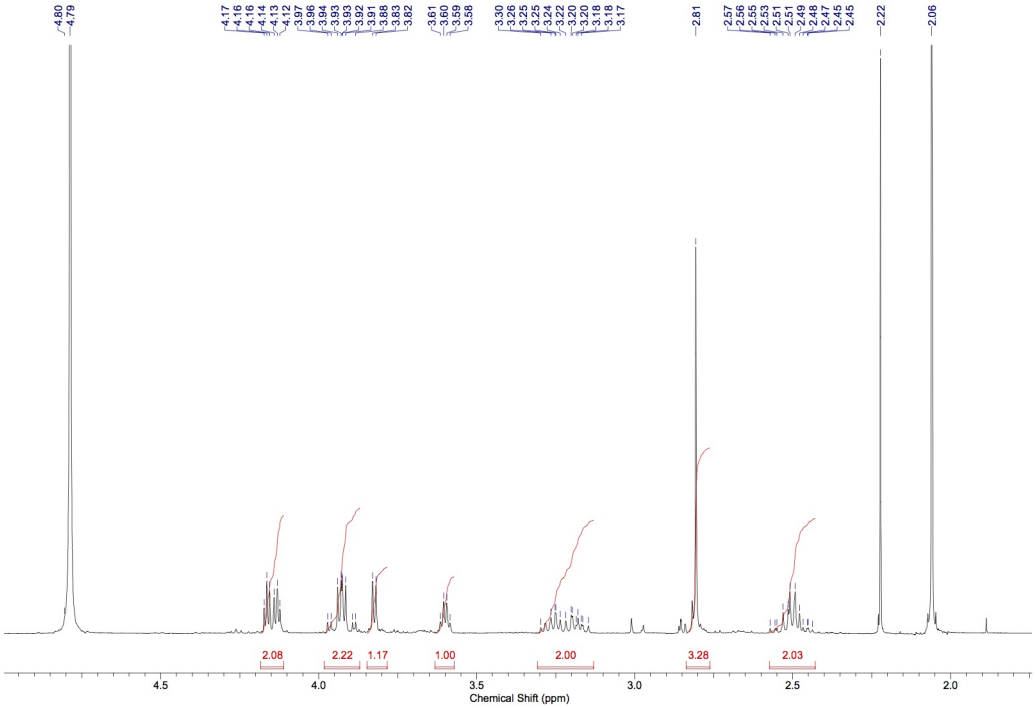

^{13}C (125.6 MHz, D_2O)

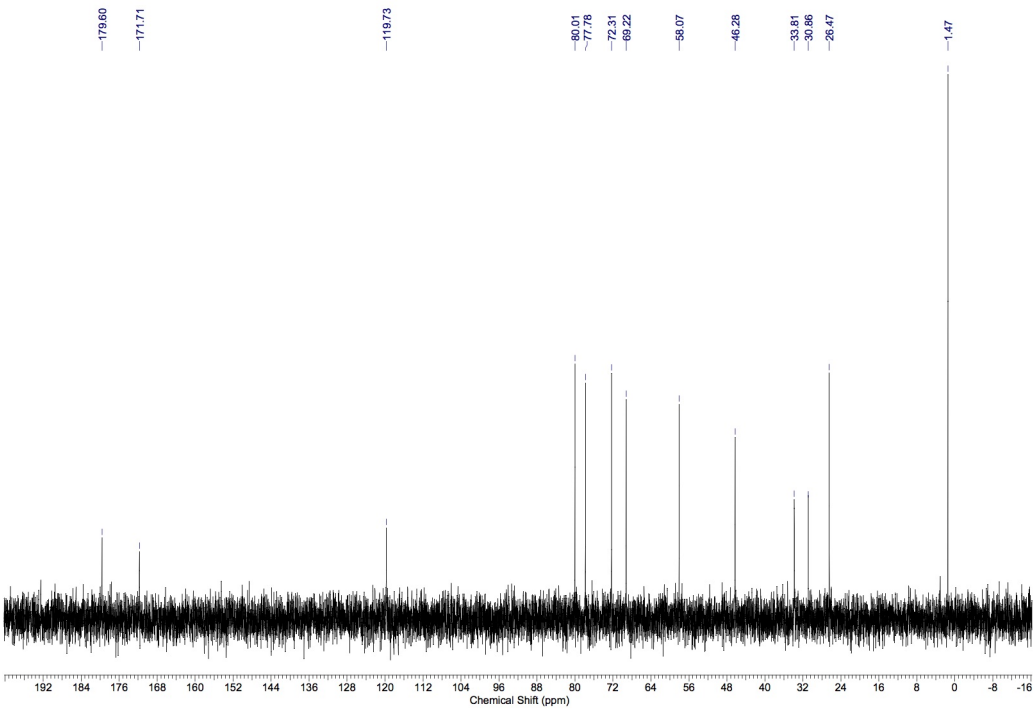

References

1. a) Y. Zhao and D. G. Truhlar, *Ther. Chem. Acc.*, 2008, **120**, 215-241; b) Y. Zhao and D. G. Truhlar, *Acc. Chem. Res.*, 2008, **41**, 157-167.

2. M. J. Frisch, G. W. Trucks, H. B. Schlegel, G. E. Robb, J. R. Cheeseman, G. Scalmani, V. Barone, B. Mennucci, G. A. Petersson, H. Nakatsuji, M. Caricato, X. Li, H. P. Hratchian, A. F. Izmaylov, J. Bloino, G. Zheng, J. L. Sonnerberg, M. Hada, M. Ehara, K. Toyota, R. Fukuda, J. Hasegawa, M. Ishida, T. Nakajima, Y. Honda, O Kitao, H. Nakai, T. Vreven, J. J. A. Montgomery, J. E. Peralta, F. Ogliaro, M. Bearpark, J. J. Heyd, E. Brothers, K. N. Kudin, V. N. Staroverov, R. Kobayashi, J. Normand, K. Raghavachari, A. Rendell, J. C. Burant, S. S. Iyengar, J. Tomasi, M. Cossi, N. Rega, N. J. millam, M. Klene, J. E. Knox, J. B. Cross, V. Bakken, C. Adamo, J. Jaramillo, R. Gomperts, R. E. Stratmann, O. Yazyev, A. J. Austin, R. Cammi, C. Pomelli, J. W. Ochterski, R. L. Martin, K. Morokuma, V. G. Zakrzewski, G. A. Goth, P. Salvador, J. J. Dannenberg, S. Dapprich, A. D. Daniels, Ö. Farkas, J. B. Foresman, J. V. Ortiz, J. Cioslowski and D. J. Fox, *Gaussian 09, Revision C.01*, Gaussian, Inc.: Wallingford CT, 2010.

3. Araújo, N.; Jenkinson, S. F.; Martínez, R. F.; Glawar, A. F. G.; Wormald, M. R.; Butters, T. D.; Nakagawa, S.; Adachi, I.; Kato, A.; Yoshihara, A.; Akimitsu, K.; Izumori, K.; Fleet, G. W. J., *Org. Lett.* **2012**, *14*, 4174-4177.

4. S. D. Boomkamp, J. S. S. Rountree, D. C. Neville, R. A. Dwek, G. W. J. Fleet and T. D. Butters, *Glycoconjugate J.*, 2010, **27**, 297-308.

5. J. P. Shilvock, R. Nash, J. D. Lloyd, A. L. Winters, N. Asano and G. W. J. Fleet, *Tetrahedron: Asymmetry,* 1998, **9**, 3505-3516.

6. I. Bruce, G. W. J. Fleet, I. Dibello and B. Winchester, *Tetrahedron,* 1992, **48**, 10191-10200.

7. C. Falentin, D. Beaupere, G. Demailly and I. Stasik, *Tetrahedron,* 2008, **64**, 9989-9991.

8. A. N. Hulme, C. H. Montgomery and D. K. Henderson, *J. Chem. Soc., Perkin Trans.,* 2000, **1**, 1837−1841.

9. G. W. J. Fleet, and D. Witty, *Tetrahedron: Asymm.* **1990**, *1*, 61, 119-136.